Tatzel, M., Dunkl, I., von Eynatten, H. (2017): Provenance of Palaeo-Rhine sediments from zircon thermochronology, geochemistry, U/Pb dating and heavy mineral assemblages. - *Basin Research*, *29*, S1, pp. 396—417.

DOI: http://doi.org/10.1111/bre.12155

Provenance of Palaeo-Rhine sediments from zircon thermochronology, geochemistry, U/Pb dating and heavy mineral assemblages

Michael Tatzel [ab], István Dunkl [b], Hilmar von Eynatten [b]

[a] German Research Center for Geosciences, GFZ Potsdam, Germany

[b] Sedimentology and Environmental Geology, Geoscience Center, University of Göttingen, Germany

Please cite this article as:

Michael Tatzel, István Dunkl, Hilmar von Eynatten

Provenance of Palaeo-Rhine sediments from zircon thermochronology, geochemistry, U/Pb dating and heavy mineral assemblages

Basin Research (2015)

doi: 10.1111/bre.12155

Abstract Sediments deposited in the Late Cenozoic basins of the Central European Rift System, including the Upper Rhine Graben (URG) and the Lower Rhine Embayment (LRE), document the drastic extension of the Rhine's catchment towards the Central Alps in the Late Pliocene by distinct heavy mineral assemblages. This outstanding change in principal sediment sources should be accompanied by a change towards distinctly younger (i.e. Tertiary) detrital mineral cooling ages. Therefore, it provides a particularly well-suited framework to explore the thermochronological provenance record in relation to heavy mineral assemblages. In this multi-proxy approach we (i) exploit and elaborate detrital zircon (U-Th)/He thermochronology (ZHe) for sediment provenance surveys, (ii) document shortcomings if only a single geochronological method is employed, and (iii) obtain tighter constraints on the sources of Paleo-Rhine sediments. Our results are based on Pliocene and Pleistocene sediment samples from the northern URG (drill core Ludwigshafen P36) and the LRE (lignite mine Hambach). In a Late Pliocene URG sample, Variscan and Permo-Triassic cooling ages dominate the age spectra of the ZHe and Zircon fission track (ZFT) thermochronometers. The youngest ages are Late Cretaceous and these zircons show rare earth element signatures that suggest derivation from hydrothermally affected basement rocks of the URG margins. In contrast, a Lower Pleistocene URG sample contains significant Tertiary age components that unequivocally indicate Alpine sources. This cardinal difference coincides well with a significant change in the heavy mineral assemblage. The extension of the catchment of the Rhine towards the Central Alps is considered to occur no earlier than the latest Pliocene (i.e. after ~3.0 Ma). Despite strongly contrasting heavy mineral compositions, the Pliocene and Pleistocene samples from the LRE show largely similar ZHe and ZFT age distributions dominated by Permo-Triassic and Variscan ages. Admixture of zircon-dominated, but overall heavy mineral-poor sediment derived from local drainages of the Rhenish Massif likely explains this apparent contradiction in sediment provenance proxies. Tertiary cooling ages occur in both Pliocene and Pleistocene LRE samples. Zircon Th/U ratios and U/Pb ages reveal that the young age component in Late Pliocene sediments from the LRE is not derived from the Alps but from Oligocene trachytic members of the Central European volcanic centres of the Vogelsberg, Westerwald, and/or Siebengebirge. The integration of ZHe and ZFT techniques with zircon geochemistry and U/Pb geochronology adds the respective advantages of each method and allows for a very detailed picture of detrital zircon provenance.

Introduction

Sediment provenance is commonly inferred from single, mineralogical, geochemical, or geochronological proxies such as heavy mineral assemblages, zircon U/Pb ages, or detrital thermochronology. Taken separately, these might, however, yield ambiguous results and compared to one another even render conflicting interpretations. We explore benefits from the combination of several methods with emphasis on detrital zircon (U-Th)/He dating in the framework of Late Cenozoic Palaeo-Rhine sediments. These are particularly well suited for such an approach as sediments from the Upper Rhine Graben (URG) and the Lower Rhine Embayment (LRE; Fig. 1) reveal a prominent transition in sediment provenance around the Pliocene-Pleistocene boundary (Boenigk, 1976, 1978a,b; Hagedorn & Boenigk, 2008; Hoselmann, 2008; Kemna, 2008a). This change is expressed in the transition from ultra-stable, ZTR-dominated (zircon, tourmaline and rutile) heavy mineral spectra towards assemblages rich in garnet, epidote and amphibole. The cause of this transition is the extension of the southern limit of the Rhine's drainage basin from the Vosges-Kaiserstuhl-Black Forest area to the Alpine realm. The tapping of new sources located in the Central Alps or in the Northern Alpine Foreland Basin (NAFB; i.e. Central Alpine material intermittently stored in the foreland) is thought to have mainly occurred in the latest Pliocene (i.e. late Piacenzian time; after ~3.0 Ma; Berger et al., 2005; Gradstein et al., 2012). Sediment transport to the URG already in early Piacenzian time (~3.6 Ma) was inferred from apatite fission track (AFT) data from Pliocene URG sediments where sediment sources at the northern margin of the Alps (i.e. in the Subalpine Molasse and/or the western Rhenodanubian Flysch) were suggested (Reiter et al., 2013). The commonly accepted picture of Alpine-derived Pleistocene Rhine sediment has recently been challenged by Krippner & Bahlburg (2013) who speculate on sources outside the Alps for Pleistocene Rhine sediments, because of the complete absence of zircons with U/Pb ages <200 Ma in Middle Pleistocene Rhine sediments.

Bedrock exposed in the modern catchment of the river Rhine is characterized by significantly different zircon low-temperature cooling ages: Oligocene-Miocene metamorphism in the Central Alps and related late Cenozoic low-temperature cooling ages (Hunziker et al., 1992; Schlunegger & Willett, 1999; Bernet et al., 2004; Glotzbach et al., 2008; Vernon et al., 2008) contrast with considerably older, pre-Alpine cooling ages in the Central European basement and its sedimentary cover (Hejl et al., 1997; Köppen & Carter, 2000; Timar-Geng et al., 2004, 2006; Karg et al., 2005; Dresmann et al., 2010).

Hence, the chronological methods most sensitive to distinguish sediment sources in a catchment comprising a young orogenic belt such as the Rhine's catchment are the zircon (U-Th)/He (ZHe) and the zircon fission track (ZFT) thermochronometers with closure temperatures (TC) of ca. 170-190°C and 240-300°C respectively (Rahn et al., 2004; Reiners et al., 2004). Their relatively low closure temperatures allow recording mid- or shallow crustal thermal events. The widely used apatite-based low-T thermochronology (AFT and AHe methods) also record near-surface thermal events, but their significantly lower closure temperatures of ca. 110°C and 70°C respectively (Naeser & Faul, 1969; Wolf et al., 1996) make AFT and AHe more sensitive to reset through sedimentary burial. This high sensitivity might decrease the probability of preserving the cooling history of the source bedrock. On the other hand,

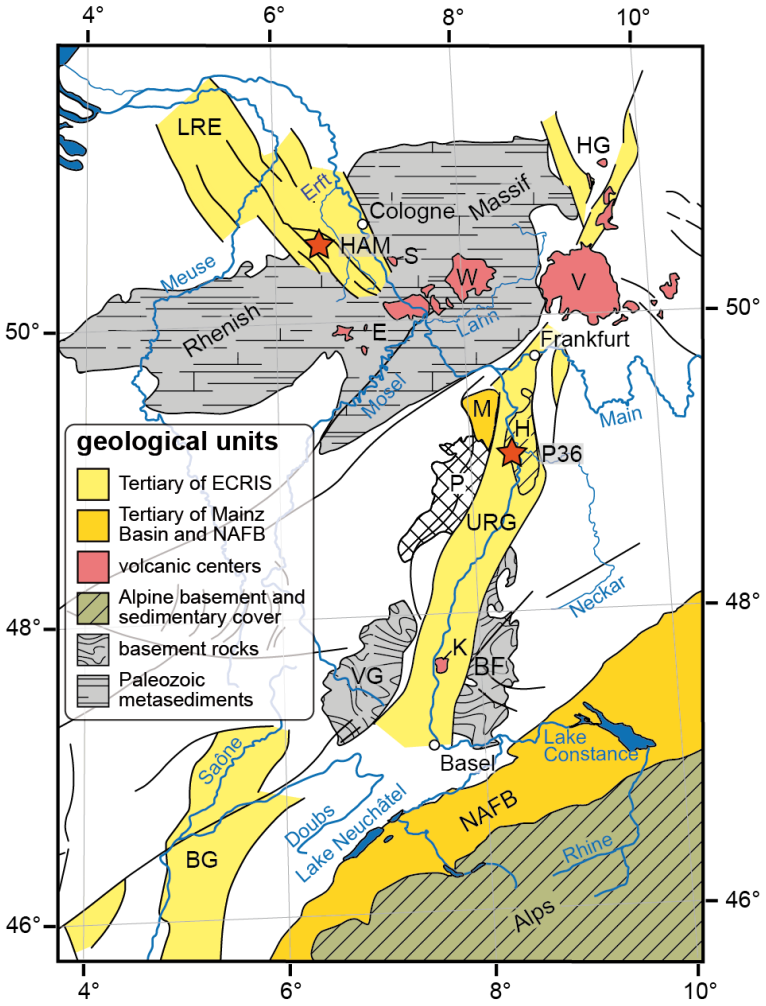

Figure 1: Simplified overview map modified after Dèzes et al. (2004) showing the European Cenozoic Rift System (ECRIS) with the Upper Rhine Graben (URG), the Lower Rhine Embayment (LRE), Hessian Grabens (HG), the Bresse Graben (BG), and simplified geological units. BF, Black Forest; E, Eifel; H, Heidelberg Basin; K, Kaiserstuhl; M, Mainz Basin; NAFB, Northern Alpine Foreland Basin; P, Pfälzerwald; S, Siebengebirge; V, Vogelsberg; VG, Vosges; W, Westerwald. Sample locations are shown as red stars.

detrital zircon U/Pb geochronology (T_C > 900°C; Cherniak & Watson, 2001) is insensitive to mid- or shallow crustal thermal events and only records crystallization and high-T metamorphic crystal growth.

Zircon fission track thermochronology has been successfully used in many sediment provenance surveys (Hurford et al., 1984; Spiegel et al., 2000, 2007; Dunkl et al., 2001; Bernet et al., 2004; Carter, 2007). The closure temperature of ZFT is higher than that of ZHe, but it similarly records the post-metamorphic cooling. The use of detrital ZFT, however, is limited because crystals with old cooling ages and/or high U-concentrations commonly have spontaneous track densities that are too high to be optically discerned and counted (Wagner, 1978). Therefore, such grains do not appear in ZFT age distributions and, consequently, such distributions might lead to false conclusions by the over-representation of the younger, that is low track density zircon grain populations. In contrast, ZHe thermochronology can record cooling events as old as several hundred Ma (Reiners, 2005) and is thus better suited to capture the entire age distribution.

To date, detrital (U-Th)/He thermochronology was applied only in a few sediment provenance studies (Rahl et al., 2003; Reiners, 2005; Horton et al., 2010) which is for two main reasons: (i) the time-consuming analysis through single-crystal degassing and chemical dissolution in pressurized vessels impede on the acquisition of statistically reasonable amounts of single-grain ages, and (ii) the unknown zoning patterns and abrasion of detrital grains through sediment transport increase uncertainties in the age calculation.

In this study, we use the provenance scenario outlined above to (i) validate the use of ZHe cooling ages in provenance studies by comparing results from detrital ZHe and ZFT dating, to (ii) note the shortcomings of single proxies in documenting sediment provenance and to (iii) gain further constraints on the Plio-Pleistocene fluvial history of the Rhine River by exploiting the full potential of the ZHe dating procedure through integrating single-crystal trace- and rare earth element (REE) analyses. Zircon U/Pb analyses are used to discern sediment sources in the Tertiary volcanic centres of Central Europe and Periadriatic volcanics from sediment sources in Alpine bedrock that cooled by Tertiary exhumation.

Geological Setting

The Upper Rhine Graben

The URG stretches in NNE-SSW direction from Frankfurt to Basel and forms a prominent limb of the European Cenozoic Rift System (Fig. 1), which is temporarily and spatially associated with volcanic activity (Ziegler, 1992). The graben formation initiated in Middle to Late Eocene times through passive rifting induced by collision-related intraplate stress (Dèzes et al., 2004) following zones of weakness within the Variscan basement (Illies, 1977; Ziegler, 1992). Contemporaneous sedimentation occurred initially under continental fluvial to lacustrine conditions, followed by major marine ingressions in the Rupelian (Berger et al., 2005). After non-deposition and/or erosion leading to hiatuses in the Early to Middle Miocene, deposition occurred in fluvial and lacustrine environments from the Late Miocene onward (Berger et al., 2005). The heavy mineral composition of Palaeo-Rhine sediments indicates that the river Rhine was established in its approximate present course since the Late Pliocene and transported Alpine debris to the URG basin (Boenigk, 1976, 1978a,b; Berger et al., 2005; Hoselmann, 2008).

Fluvial, quartz-rich, non-calcareous, kaolinitic, greyish to whitish sands and partly humic, fine-grained sediments characterize the Pliocene Iffezheim Formation (Ellwanger et al., 2010). Heavy mineral assemblages are dominated by zircon, rutile-anatase and tourmaline, whereas individual beds also bear less stable heavy minerals. This finding is explained by erosion in local catchments of highlands along the URG (e.g. Vosges, Black Forest, Pfälzerwald). , a possible influence from Alpine sources is discussed in Gabriel et al. (2013) and Reiter et al. (2013). The latter propose sources in the Subalpine Molasse and/or the western Rhenodanubian Flysch based on detrital AFT ages.

The Pleistocene Viernheim Formation (Hoselmann et al., 2010) is characterized by dominantly well-sorted, fine- to medium sized, greenish to greyish sands with some silty to clayey beds (Gabriel et

al., 2013). Alpine provenance is indicated by notable fractions of muscovite, high carbonate contents, instable heavy mineral spectra dominated by garnet, hornblende, and epidote (Hagedorn & Boenigk, 2008; Hoselmann, 2008), and Late Miocene AFT age components (Reiter et al., 2013). In the Ludwigshafen area, i.e. at the western margin of the URG-internal Heidelberg Basin (Fig. 1), the sedimentary succession is discontinuous through intercalations of local alluvial fans of non-carbonaceous material derived from the Pfälzerwald, i.e. the Buntsandstein-dominated western margin of the northern URG (Gabriel et al., 2013; Fig. 1).

In drill core P34, which is located only a few hundred metres from drill core P36 investigated here, a magnetic polarity reversal, which likely represents the Gauss- Matuyama reversal (2.59 Ma; Pliocene to Pleistocene boundary according to Gradstein et al., 2012), was found at the same depth where the heavy mineral composition significantly changes (Rolf et al., 2008; Scheidt et al., 2015). Thus, in the northern URG the Plio-Pleistocene boundary is approximately delineated by the lithostratigraphic units Iffezheim Formation and Viernheim Formation.

The Lower Rhine Embayment

The LRE extends from the northwest into the Rhenish Massif (Fig. 1). It is segmented into numerous tectonic blocks running parallel to the regional NW-SE aligned stress field (Illies, 1977). Distribution and thickness of sediments are dominantly governed by the individual subsidence histories of these tectonic blocks (Kemna, 2008b). Major subsidence since the Middle Oligocene led to the transgression of the North Sea. Shoreline retreat was followed by regression in the Middle Miocene and lead to the formation of fluvial gravel, sand, clay, and marsh deposits, the precursors of the up to 100 m thick brown lignite deposits that are exploited in three open cast mines today (Walter, 2010). During the Pliocene, the Palaeo-Rhine, the East Meuse, the Palaeo-Erft (both Meuse and Erft rivers drain the Rhenish Massif and Eifel towards the North into the LRE, Fig. 1), deposited yellowish to whitish quartz sands, and small- to medium sized gravels into a large near-shore alluvial fan system (Kemna, 2005) named Kieseloolite Fm. In the Upper Pliocene, mostly bluegreen coloured, fine-grained sediments, termed Reuver Clay, were deposited throughout most of the LRE area. The Upper Reuver Clay, also referred to as the Öbel beds, frequently contains sandy layers in incised channels and is assigned to the uppermost Pliocene (Boenigk & Frechen, 2006; Westerhoff et al., 2008). The Lower Pleistocene of the middle LRE area encompasses the Holzweiler Fm. that has been deposited by the East Meuse, and sediments of the Hambach beds (Kemna, 2005) which were transported by the Palaeo-Erft, a local river that has presumably drained the Eifel area (Kemna, 2008b; Fig. 1). The Hambach beds have a lithofacies characterized by extremely high quartz contents and a very stable heavy mineral composition dominated by zircon. Throughout the Middle Pleistocene, the Rhine increasingly drained through the southern part of the LRE, depositing sediments of the Upper Terrace Sequence (Niederrhein-Hauptterrassen Formation). Their lower part is termed Frechen beds and is intercalated with the Hambach beds, indicating that their deposition initiated already in the Early Pleistocene (Kemna, 2008a).

The extension of the catchment area of the river Rhine towards the Alpine realm is also recorded by Palaeo- Rhine sediments of the LRE. A change in sediment petrography in the Upper Reuver Clay, i.e. the Öbel beds, and the location of the Gauss-Matuyama reversal some metres above the Öbel beds in the open cast mine Hambach (Kemna, 2005) suggest that the breakthrough occurred in the latest Pliocene in agreement with results from the URG

Synopsis of low-temperature thermochronological data from the Rhine catchment

In this compilation, we only discuss source rocks that potentially deliver zircon to the Plio-Pleistocene river Rhine. Principally, three major domains that contribute to (Palaeo-)Rhine sediments must be distinguished: (i) the Central European platform composed of Caledonian and Variscan deformed crust and a variable sedimentary cover, reflecting the complex Mesozoic to Cenozoic evolution of this domain (Ziegler & Dèzes, 2005; Littke et al., 2008), (ii) the Alpine orogenic belt (Frey et al., 1999) and (iii) the NAFB that has stored material eroded from the Alps between Early Oligocene and Miocene (Schlunegger et al., 1997; von Eynatten, 2003).

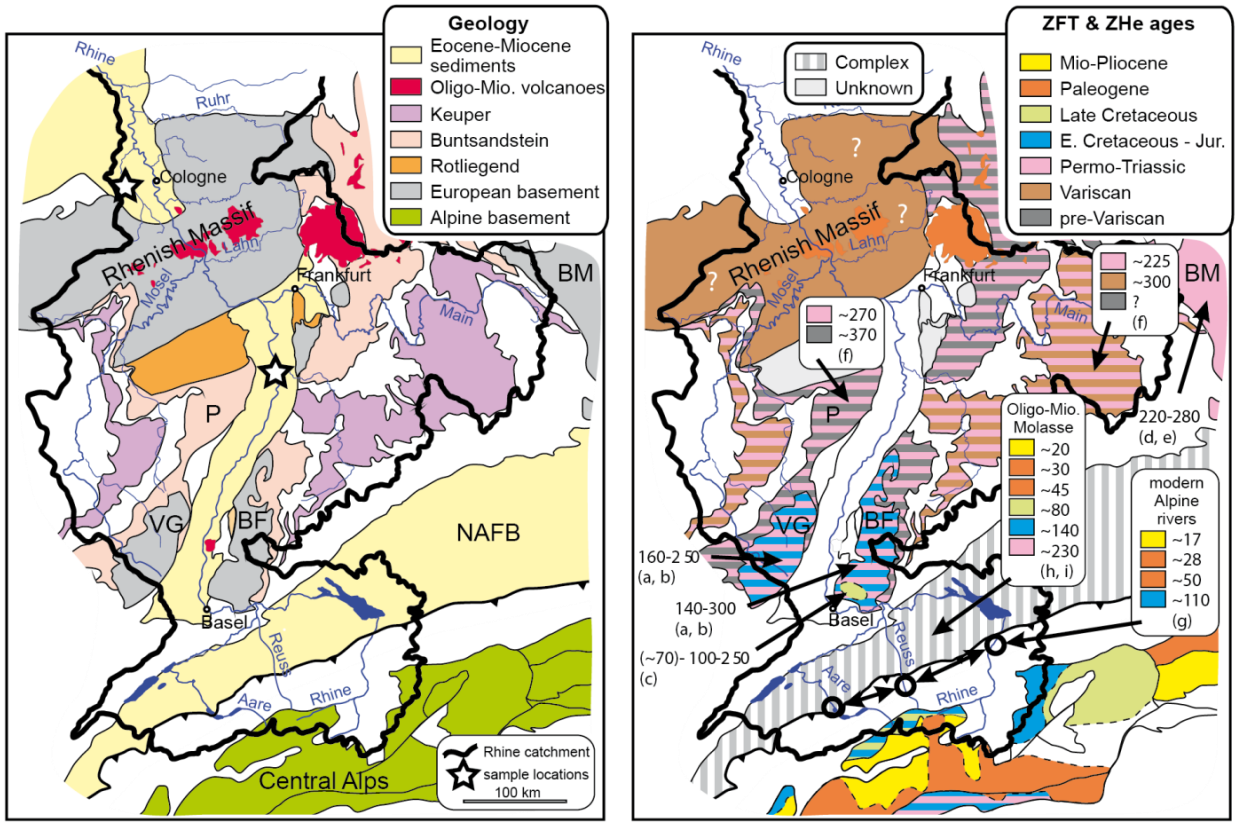

Figure 2: (a) Simplified geological map of the Rhine catchment and adjacent areas. Only zircon-bearing units are indicated. BF, Black Forest; BM, Bohemian Massif; NAFB, Northern Alpine Foreland Basin; P, Pfälzerwald; VG, Vosges. (b) Compilation of zircon low temperature thermochronological data (mostly ZFT; ages in Ma) from zircon yielding formations of the river Rhine catchment. The available ZFT (a - h) and ZHe (i) data do not fully cover all source formations. Therefore, in many cases the areas or units shown to be homogeneous are interpreted and extrapolated from relatively scarce thermochronological data. Black circles indicate ages determined in modern sediments from Alpine rivers (Bernet et al., 2004). The ZFT age contours from the Central Alps are from Vernon et al. (2008). Thermochronological data are taken from: (a) Timar-Geng et al., 2004; (b) Timar-Geng et al., 2006; (c) Dresmann et al., 2010; (d) Hejl et al., 1997; (e) Thomson & Zeh, 2000; (f) Köppen & Carter, 2000; (g) Bernet et al., 2004; (h) Spiegel et al., 2000; (i) Miller, 2012.

(i) In the Rhine catchment the Central European basement is exposed in several low- to medium mountain ranges such as the Rhenish Massif or the Black Forest (Fig. 2a). The degree of metamorphism, the dominant lithology, the post-Variscan thermal history, as well as the zircon content are variable in all these basement outcrop areas (McCann, 2008). The basement rocks exposed next to the URG in the Vosges and the Black Forest were thermally overprinted through intense Jurassic to Early Cretaceous hydrothermal activity (see compilation in Wetzel et al., 2003) that reached temperatures up to 280-330°C (Timar-Geng et al., 2004, 2006; Dresmann et al., 2010). A second thermal pulse, constrained by late Cretaceous to Palaeogene AFT ages is thought to be related to Cenozoic rifting of the URG. Temperatures did not exceed 120-150°C and thus, the ZFT and ZHe ages remained unaffected (Timar-Geng et al., 2006; Dresmann et al., 2010). Neogene uplift of the graben flanks has led to exhumation of basement rocks and created relatively high relief in the Vosges - Black Forest area, leading to locally increased sediment generation. Further north, the Rhenish Massif is dominantly composed of Late Palaeozoic slates, i.e. zircon-poor formations. The presence of some sandstone members, however, suggests that minor amounts of detrital zircons are emitted by erosion (Walter, 2007). The post-Variscan cooling history of the Rhenish Massif is constrained by comparatively old AFT ages (i.e. between 140 and 290 Ma; Glasmacher et al., 1998; Karg et al., 2005), implying that ZHe and ZFT cooling ages in the Rhenish Massif should not be younger than Variscan or Permo-Triassic. Senglaub et al. (2005) also reported Variscan ZFT ages as old as 300-340 Ma from the northern, buried continuation of the Rhenish Massif. From the Bohemian Massif, which is exposed along the easternmost margin of the Rhine catchment and drained by the river Main, mainly Permo-Triassic ZFT ages are reported (Hejl et al., 1997; Fig. 2b).

The Mesozoic sedimentary cover contains two stratigraphic units that are potential sources of zircon grains for Rhine sediments: the Buntsandstein (Early Triassic) and the Keuper (Late Triassic) (Fig. 2a). The latter is thinner and poorer in arenite members, implying a lower zircon yield from Keuper sandstones and thus minor importance compared to the Buntsandstein (Doornenbal & Stevenson, 2010); however, both formations cover large areas in Central to Western Europe. These two units have principally different origins: (i) the Buntsandstein is derived from the south, where at that time Variscan consolidated units formed uplands such as the Bohemian Massif, the Vindelizian High (Southern Germany, Austria, Switzerland), and/or the Massif Central to Montagne Noir (France; Ziegler, 1990), whereas (ii) the Keuper is derived from the north (i.e. Scandinavia; Wurster, 1964; Paul et al., 2009). ZFT ages of Triassic sandstones from several locations within the Rhine's catchment yield Variscan and Permo-Triassic ZFT ages (Köppen & Carter, 2000). In the Buntsandstein, the dominant age component is 270 ± 9 Ma (~80%) and a minor component yields 371 ± 29 Ma (~20%). In the Keuper, ZFT age distributions show principal age components between ~225 and ~310 Ma with the youngest significant age component at 224 ± 15 Ma.

Remarkably, one Keuper sample from Poland contains detrital ZFT ages older than 400 Ma (Köppen & Carter, 2000). Although not located in the Rhine catchment these data indicate the presence of pre-Variscan ZFT cooling ages even in Triassic strata of the Central European platform.

Because of the large areal extent of epicontinental Late Permian to Mesozoic sedimentary rocks and the lack of ZHe analyses from these formations, we performed some pilot analyses from Permian (Rotliegend) andTriassic (Keuper) sandstone samples. Although the number of aliquots is low, these data serve as a preliminary orientation to supplement the ZFT data introduced above and provide further constraints to possible post-depositional thermal events. Results from the Rotliegend sample (V-35, derived from the NE margin of the Rhine catchment; Table 1) yield ZHe ages close to or older than the age of deposition (i.e. 329-294 Ma; Table 2). These data are consistent with the ZFT data and therefore a significant thermal reset is unlikely. The ZHe ages from a Keuper sandstone sample (DX-8, Table 1) are younger than the ZFT ages reported by Köppen & Carter (2000) and are even slightly younger than the age of deposition (210-172 Ma; Table 2). This suggests that the South German Keuper has experienced a moderate thermal overprint and is hence expected to deliver dominantly latest Triassic to early/mid Jurassic ZHe ages.

(ii) The Alps emit zircons with overall significantly younger fission track- and He cooling ages than the Central European platform. However, the Alpine part of the Rhine's catchment area is rather complex in terms of thermochronology (Fig. 2b). The Lepontine metamorphic dome experienced pronounced Neogene exhumation (Hurford, 1986) and yields the youngest, Pliocene, bedrock ZFT ages. Older Tertiary bedrock cooling ages are found where higher levels of the tectonostratigraphic pile are preserved through less deep Cenozoic erosion (Vernon et al., 2008). Late Cretaceous ZFT ages are frequent in the cover nappes and in the Austroalpine domain including the Ötztal and Silvretta basement nappes (Elias, 1998; Spiegel et al., 2000; Brügel et al., 2003), and along the northern margin of the Aar Massif where also Jurassic ZFT cooling ages were reported (Hurford et al., 1989; Michalski & Soom, 1990). The spatial distribution of bedrock cooling ages in the Central Alps as derived from a compilation of ZFT ages by Vernon et al. (2008) is displayed in Fig. 2b.

Modern, Alpine-derived Rhine sediment shows characteristic ZFT age components around ~17 Ma, ~28 Ma, ~50 Ma and ~90 to 130 Ma (Bernet et al., 2004; black circles in Fig. 2b). The youngest age components that are ascribed to the rapidly exhuming Central Alps (i.e. the eastern Aar- and Gotthard Massifs) are the dominant age components in sediments from the headwaters of the Rhine (Buchs River ~17 Ma: 41%, ~30 Ma: 49%; Reuss River: ~17 Ma: 85%, ~30 Ma: 10%; Aare River: ~17 Ma: 90%, ±30 Ma: not present).

(iii) The NAFB records the erosion history of the Alps from Early Oligocene to Middle Miocene times. The older members of the foreland basin succession contain higher proportions of pre-Cenozoic ZFT and ZHe ages compared to the Miocene members and the modern Alpine river sediments (Spiegel et al., 2000; Miller, 2012). Age spectra of Miocene strata are dominated by zircon cooling ages around 40- 30 Ma. Molasse sandstones have a relatively high erodibility and are frequently mobilized and redeposited across the Molasse Basin by the Rhine River and its tributaries (Burkhard, 1990).

Materials and methods

We collected five samples from drill core P36 from Ludwigshafen, which is situated at the western edge of the Heidelberg Basin (Fig. 1); two from the Pliocene Iffezheim Fm. (P36-1, P36-2), and two from the Pleistocene Viernheim Fm. (P36-3, P36-5; Table 1). One sample (P36-4) represents local alluvial fans that are most probably derived from the Buntsandstein- dominated western URG shoulder (Pfälzerwald; Fig. 1) and intercalated into the Pleistocene beds. Chronostratigraphic ages of the samples are inferred from (i) magnetostratigraphy of drill core P36 (Scheidt et al., 2015) for the Viernheim Fm., and (ii) correlations to the nearby (<500 m) borehole P34 for the Iffezheim Fm. (Gabriel et al., 2013; Reiter et al., 2013): samples P36-1 and P36-2 were deposited at ~3.2- 3.0 Ma, P36-3 at ~2.6-2.3 Ma, P36-4 at ~1.4-1.1 Ma and P36-5 at 1.0-0.8 Ma.

We collected six samples from sediments overlying the lignite-bearing strata of the lignite mine Hambach, located 40 km West of Cologne in the LRE. Unconsolidated sand of the Kieseloolite Fm. (HAM-1, HAM-2) is overlain by a sandy channel fill of the Öbel beds (HAM- 3). Light-coloured sands of the Hambach beds (HAM-5) were found intercalated between the Frechen beds (HAM-4) and the Upper Terrace Sequence (HAM-6; Table 1). ZHe and ZFT analyses were carried out on two URG and two LRE samples (P36-1, P36-5, HAM-1 and HAM-4); for each location one Pliocene and one Pleistocene sample was selected (see below). Magnetostratigraphic constraints to provide precise chronostratigraphic ages are not available in Hambach. Samples HAM-1 and HAM-2 are Late Pliocene in age, HAM-3 is from the latest Pliocene, HAM-4 and HAM-5 are Early Pleistocene and HAM-6 is Mid Pleistocene in age.

Table 1: Locations and stratigraphic positions of samples from drill core Ludwigshafen Parkinsel P36 and open cast mine Hambach

Drill core Ludwigshafen Parkinsel P36 (Upper Rhine Graben)

sample	latitude	longitude	depth [m]	stratigraphy	age	references
P36-5	49°28'8.85"	8°27'41.70"	83.5 - 83 (*below 90 m a.s.l.)	Viernheim Formation	Early Pleistocene	Weidenfeller & Knipping (2008)
P36-4	''	''	111.9 - 111.3	Viernheim Formation	Early Pleistocene	Rolf et al. (2008)
P36-3	''	''	180.0 to 179.7 + 179.0 to178.7	Viernheim Formation	Early Pleistocene	Weidenfeller & Kärcher (2008)
P36-2	''	''	251.2 to 251.0 + 250.6 to 250.4	Iffezheim Formation	Late Pliocene	
P36-1	''	''	259.4 to 259.2 + 258.25 to 258.0	Iffezheim Formation	Late Pliocene	

Open cast mine Hambach (Lower Rhine Embayment)

sample	latitude	longitude	elevation [m, a.s.l.]	stratigraphy	age	reference
HAM-6	50°53'7.10"	6°31'21.32"	56 ± 4	Upper Terrace Sequence (base)	Mid Pleistocene	Kemna (2008a)
HAM-5	50°55'9.95"	6°34'20.8"	23 ± 5	Hambach beds	Early Pleistocene	
HAM-4	50°55'10.29"	6°34'17.48"	20 ± 5	Frechen beds	Early Pleistocene	
HAM-3	50°53'37.40"	6°32'16.25"	ca. 24	Öbel beds	latest Pliocene	
HAM-2	50°53'13.59"	6°31'32.39"		Kieseloolite Formation	Late Pliocene	
HAM-1	50°53'7.10"	6°31'21.32"	40 ± 4	Kieseloolite Formation	Late Pliocene	

Keuper sample from Heilbronn Quarry Jägerhaus (sampled by J. Paul)

sample	latitude	longitude	elevation [m, a.s.l.]	stratigraphy	age	reference
DX-8	49°8'9.69"	9°16'10.62"		Stuttgart Formation	Carnian (T3)	Paul et al. (2009)

Lover Permian pilot sample from a borehole (sampled by V.-E. Hoffmann)

sample	latitude	longitude	elevation [m, a.s.l.]	stratigraphy	age
V-35	52°38'44.2"	11°35'56"	-3800	Rotliegend	L. Permian

Heavymineral analysis

The samples were wet sieved for the size fraction 63-125 µm, and carbonate was dissolved using 5% acetic acid for 2-6 days depending on sample reactivity. Following density separation by sodium polytungstate set to 2.85-2.90 g cm^{-1}, the dense fraction was immersed in Meltmount (n= 1.66) on a glass slide and sealed with a cover glass. Heavy mineral quantification by the ribbon counting method (Mange & Maurer, 1992) using a ZEISS axioplan polarizing microscope is based on at least 200 translucent grains. Composite grains, carbonates, iron oxides, chlorite, and ambiguous altered minerals (referred to as alterite in previous studies, Boenigk, 1978b; Hagedorn & Boenigk, 2008; Hoselmann, 2008) have been excluded from counting. Heavy mineral indices used to discriminate sediment sources are based on counts of translucent minerals: (i) GZi = garnet * 100/ (garnet + zircon) (Morton & Hallsworth, 1994), and (ii) ZTR = (zircon+ tourmaline + rutile)/(sum of all translucent grains except anatase and brookite).

Zircon (U-Th)/He thermochronology and trace element geochemistry

Zircon grains were randomly selected and checked for inclusions using a polarizing microscope. Single zircon aliquots were transferred into Pt microcapsules and degassed by IR laser heating. Details of the analytical procedure are described in the methodical supplement of Hetzel et al. (2011). Dissolution was accomplished by distilled 48% hydrofluoric (HF) and 65% nitric acid (HNO3) (10 : 1) at 220°C in pressurized vessels for five days. The concentrations of U and Th were determined by isotope dilution, whereas Sm, Zr and a set of other 32 chemical elements including REEs were determined by external calibration using a Perkin Elmer Elan DRC II ICP-MS equipped with an APEX micro-flow nebulizer at the Geoscience Center of the University of Göttingen. The raw zircon (U-Th)/He ages were corrected for alpha-particle ejection (FT correction) after Farley et al. (1996) and Hourigan et al. (2005), assuming a homogenous distribution of U, Th and Sm in the crystals. The FT correction was also applied to rounded crystals, because the presence of euhedral grains with well-preserved faces and edges indicates insignificant abrasion following erosion. The total analytical uncertainty (TAU) was calculated by Gaussian propagation of uncertainties of the He determination and the weighted uncertainties of U, Th and Sm measurements. The uncertainty of ZHe ages were estimated by adding uncertainties on the FT correction factor and TAU values. To warrant accuracy, we regularly analyse the Fish Canyon zircon age standard that has an Ar/Ar-based eruption age of 28.01 ± 0.04 Ma (Phillips & Matchan, 2013). Our longterm average Fish Canyon ZHe age is 27.8 ± 0.3 Ma (1 SE, n= 99), which is within uncertainty identical to the Ar/Ar age. Zonation of parent nuclides within the crystals may lead to biased ages (Hourigan et al., 2005), however, the majority of zircons analysed is likely not affected by such effects as revealed by a dominantly homogenous distribution of fission tracks.

The number of dated zircon crystals (30-33) allows tracking the expected major contrast in apparent ZHe age signatures between Late Pliocene and Early Pleistocene Palaeo-Rhine sediments due to the strongly increased sediment mass fluxes through the connection of the Central Alps to the Rhine's catchment.

Zircon fission track thermochronology

Zircon crystals were embedded in PFA Teflon and two crystal mounts were produced from each sample. These mounts were diamond polished using a five-step procedure. To reveal the spontaneous tracks in zircon grains, a eutectic melt of NaOH-KOH at 225°C was used (Gleadow et al., 1976) where the etching time varied from 21 to 54 h. Neutron irradiations were performed applying the external detector method (Gleadow, 1981) in the nuclear reactor at Oregon State University. After irradiation the induced fission tracks in the mica detectors were revealed by etching in 40% HF for 30 min. Tracks were counted using a ZEISS-Axioskop microscope - computer-controlled stage system (Dumitru, 1993), with a magnification of 1000. The external shape (i.e. euhedral vs. rounded) of each dated zircon has been documented during the microscopic work. ZFT ages were determined by the zeta method (Hurford & Green, 1983) using age standards listed in Hurford (1998). The error was estimated according to Green (1981); calculations and plots were made using the software 'TRACKKEY' (Dunkl, 2002).

Zircon U/Pb geochronology

U/Pb analyses by laser-ablation ICP-MS were carried out on selected, euhedral zircon crystals from samples P36-5 and HAM-1. The zircon crystals were embedded in epoxy resin and polished (using 9, 3 and 1 µm diamond suspensions). U/Pb dating was performed using a Resonetics excimer laser coupled to a Thermo Scientific Element 2 ICP-MS at the Geoscience Center of the University of Göttingen following the method of Frei and Gerdes (2009). The diameter of the laser beam was 33 lm and the ablation time 25 s. Drift- and fractionation correction was done by standard-sample bracketing using the GJ-1 zircon reference material (Jackson et al., 2004). Accuracy was verified by analyses of two secondary standards, the Plešovice zircon (Sláma et al., 2008) and the 91500 zircon (Wiedenbeck et al., 1995).

Identification of age components

The age distributions of the ZHe and ZFT data are presented by probability density plots (Hurford et al., 1984) generated using Age Display (Sircombe, 2004). Kernel density estimates were calculated according to Vermeesch (2012). We used the software 'PopShare' (Dunkl & Székely, 2002) to identify the most significant age components from the rather wide distributions of single-grain ages. Age components were identified by the Simplex procedure through minimizing the residuals, and assuming that the individual age components have Gaussian distributions.

Results

The Upper Rhine Graben

Pliocene sediments (samples P36-1 and P36-2) as well as the Pleistocene sample P36-4 (Fig. 3) are characterized by heavy mineral spectra dominated by zircon, tourmaline and TiO_2- polymorphs. Lower- and Middle Pleistocene Rhine sediments are characterized by garnet, amphibole and epidote-group minerals and thus have low ZTR and high GZi values (P36-3 and P36-5; Fig. 4). These samples bear high amounts of heavy minerals (8.9% and 13.7% respectively) compared to the Pliocene samples (0.4%; Fig. 2).

In the Pliocene sample P36-1, the majority of the low-T zircon ages belong to the Permo-Triassic age component (88% ZHe, 98% ZFT; Tables 3 and 4, Fig. 5). Six grains yield ages >300 Ma (Table 2). Four Cretaceous ZHe ages (between 141 and 66 Ma) are the youngest cooling ages of this sample. Three of these have higher abundances of the mid-REE compared to all other crystals, which bear typical zircon REE patterns (Fig. 7a) and comparatively low total REE concentrations (Fig. 7b).

In contrast, the Pleistocene URG sample P36-5 reveals predominantly Tertiary ZHe ages (73%) ranging between 40 and 8 Ma, with distinct Oligocene to Late Miocene age groups (32, 16, and 9 Ma; Fig. 4, Table 4). Three zircons have Late Cretaceous ZHe ages of 84-69 Ma. Only a few crystals have Carboniferous to Jurassic ages (17%). The single, very old ZHe age (Table 2) is most likely highly biased due to zoning or undetected inclusions. The chi-square statistics failed in case of all ZFT samples; this, and the high dispersion (Galbraith and Laslett, 1993) indicate that the ZFT single-grain age distributions have a polymodal character, and therefore the average ages of these samples are meaningless. The youngest ZFT age components of 32 and 17 Ma are similar to two of the Tertiary ZHe age components of 32 and 16 Ma (Fig. 5, Table 4). The U/Pb ages (n= 55) cover Palaeoproterozoic to Late Palaeozoic time and range from 2184 to 264 Ma (Table S1).

The Lower Rhine Embayment

Pliocene samples from the LRE have heavy mineral spectra dominated by zircon, tourmaline and TiO_2-polymorphs (HAM-1, HAM-2 and HAM-3), whereas Pleistocene samples (HAM-4 and HAM-6) are characterized by a dominance of garnet, amphibole and epidote group minerals (Fig. 3). Absolute amounts of heavy minerals are higher in Pleistocene sediments (0.8% and2.4%) compared to Pliocene sediments (0.1-0.2%). Sample HAM-5 is overall poor in heavy minerals (0.1%) and has an ultra-stable heavy mineral composition dominated by zircon (>80%). Samples HAM-1, HAM-2, HAM-3 and HAM-5 are characterized by high ZTR and low GZi values, whereas samples HAM-4 and HAM-6 are clearly discriminated by low ZTR and intermediate to high GZi values (Fig. 4).

Similar to the URG, the ZHe and ZFT age distributions from the Pliocene LRE sample (HAM-1) reveal prominent Permo-Triassic age components, although proportions are smaller (77% and 62% respectively; Fig. 5, Table 4). However, in contrast to the URG, significant proportions of Cenozoic

zircon cooling ages are present in both the ZHe (14%) and the ZFT (32%) age spectra. Crystals with Mid-Eocene to Oligocene ZFT ages are typically euhedral, and the older grains are mostly rounded (Fig. 6). Besides pre-Mesozoic U/Pb ages, a significant proportion (51%) of the dated zircons of sample HAM-1 (n= 45) yielded Cenozoic ages (Table S1).

The Pleistocene LRE sample (HAM-4) also yields broad Carboniferous to Early Cretaceous age components that comprise most of the dated zircons (ZHe 76%, ZFT 89%, Table 4, Fig. 5). Six crystals reveal Jurassic to Early Cretaceous ZHe ages that range from 190 to 121 Ma. Cenozoic ages are present, however, for ZFT in smaller proportion (11%) compared to the Pliocene LRE sample (32%). Three crystals define a small early Tertiary ZHe age component (63-49 Ma). Four crystals reveal Miocene ZHe ages (18.4, 10.5, 10.2 and 9.9 Ma), very similar to the youngest ZHe ages observed in the Pleistocene sample of the URG. Zircons with high REE concentrations occur exclusively in the age range from 150 to 65 Ma (Fig. 7b).

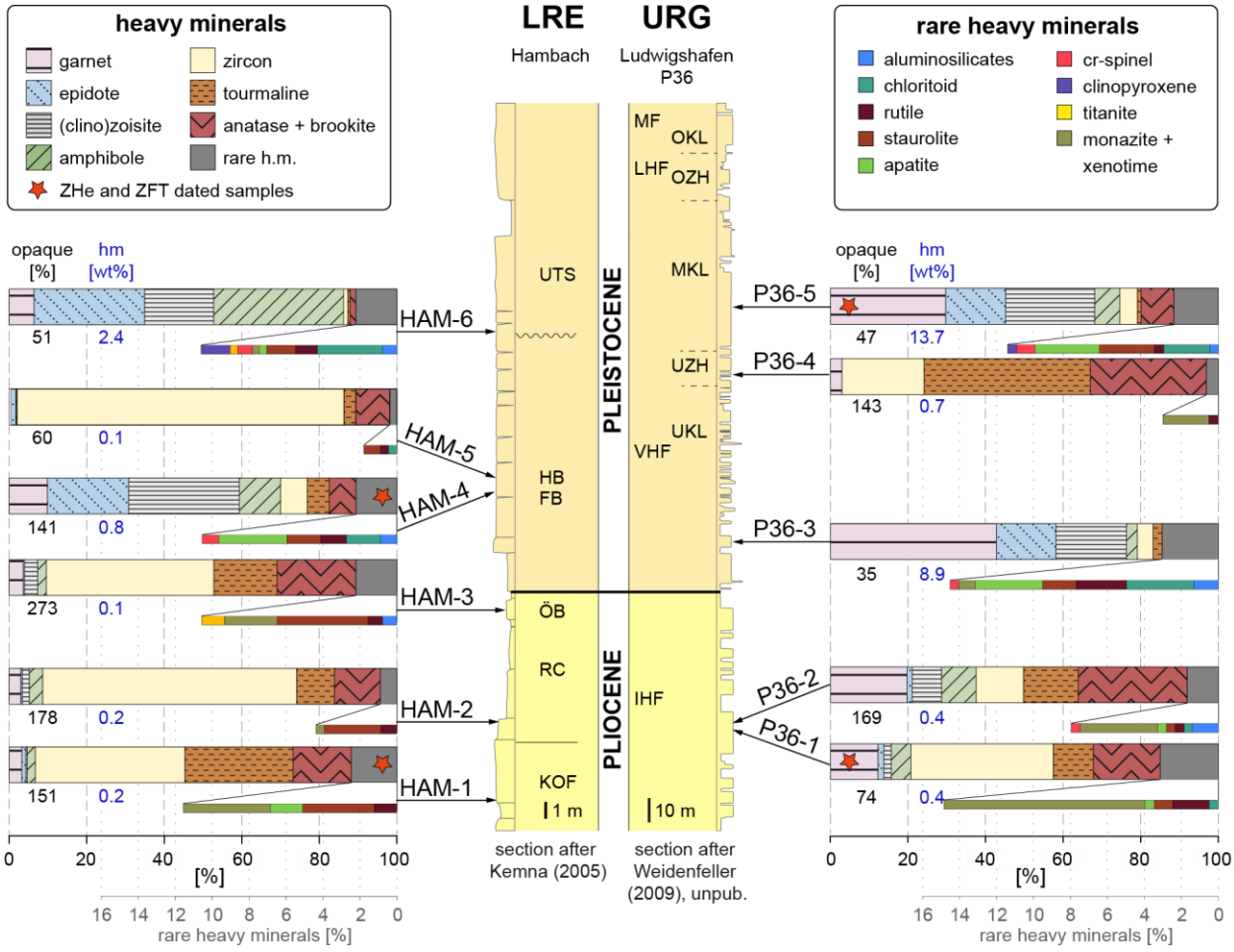

Figure 3: Stratigraphic positions and heavy mineral compositions of Pliocene and Pleistocene Palaeo-Rhine sediments from the open cast mine Hambach in the Lower Rhine Embayment (LRE) and drill core P36 from the northern Upper Rhine Graben (URG). Relative amounts of opaque minerals [%] and heavy minerals [wt%] are indicated below each sample. Lower Rhine Embayment: KOF, Kieseloolite Formation; RC, Reuver Clay; ÖB, Öbel Beds; FB, Frechen Beds; HB, Hambach Beds; UTS, Upper Terrace Sequence; Upper Rhine Graben: IHF, Iffezheim Formation; VHF, Viernheim Formation; LHF, Ludwigshafen Formation; MF, Mannheim Formation; UKL, Unteres Kieslager; UZH, Untere Zwischenhorizonte; MKL, Mittleres Kieslager; OZH, Obere Zwischenhorizonte; OKL, Oberes Kieslager.

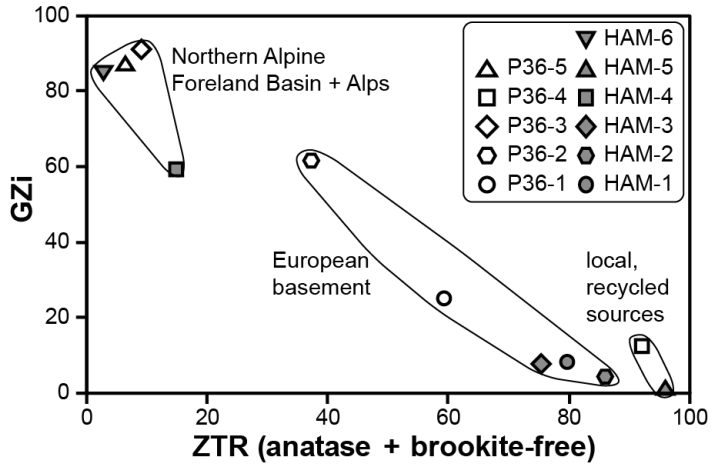

Figure 4: Major features of the heavy mineral composition of Palaeo-Rhine sediment samples displayed by the proportion of ultrastable minerals (ZTR) to the garnet-zircon index (GZi, Morton & Hallsworth, 1994). The European basement including its Permo-Mesozoic sedimentary cover yields sediment with relatively high ZTR and low GZi, whereas the Northern Alpine foreland basin and the Alps deliver immature sediment characterized by a low ZTR and high GZi. Sediment derived from local, recycled sources is extremely matured and has the highest ZTR.

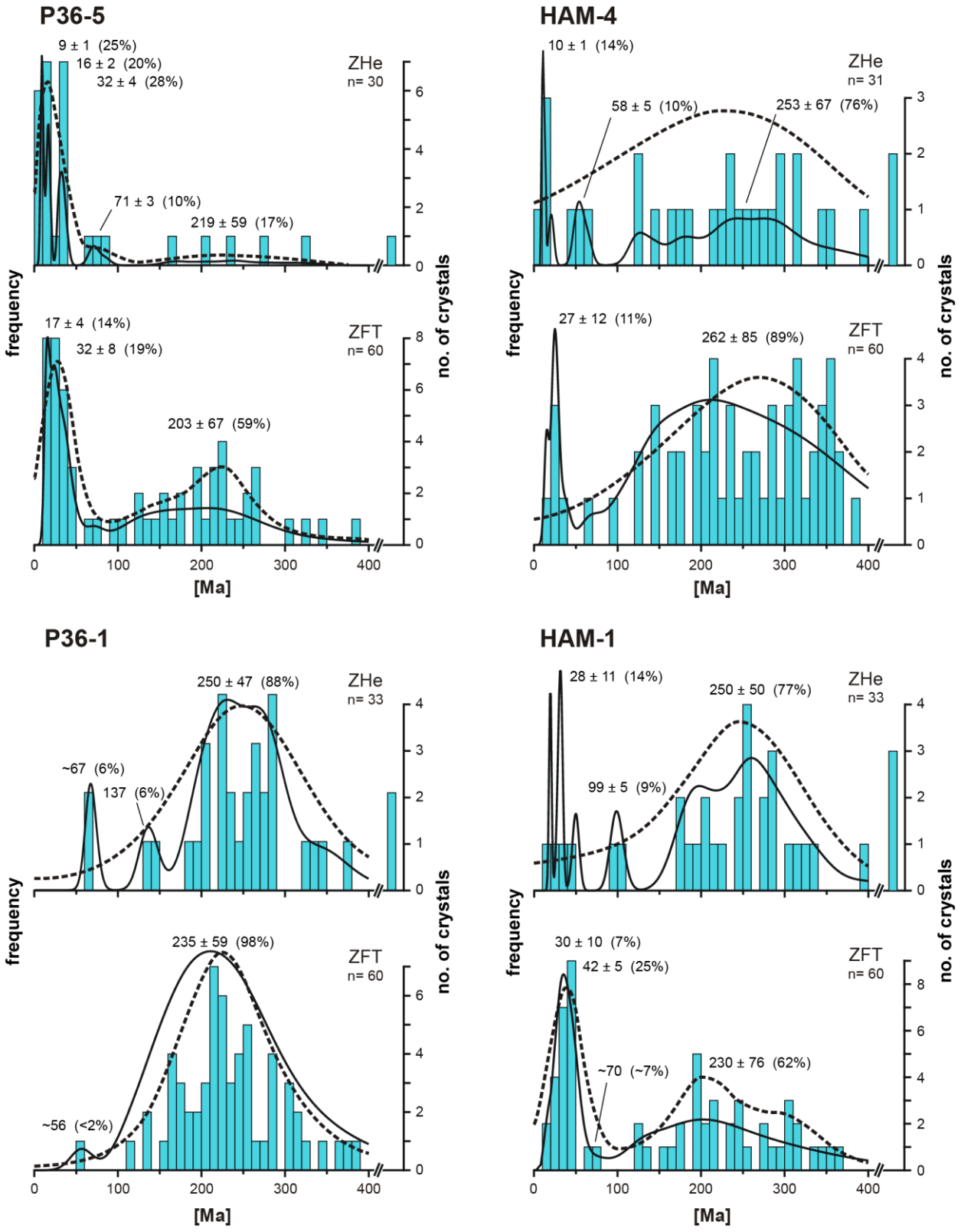

Figure 5: Zircon (U-Th)/He and fission track single-grain age distributions (by Age Display, Sircombe, 2004). The probability density curves (solid lines) and the kernel density estimates (dashed lines) are calculated according to Hurford et al. (1984) and Vermeesch (2012), respectively. The bin-width is 10 Ma in all plots; 'n' indicates the number of dated grains. Peak ages refer to age components derived from probability density plots (Hurford et al., 1984). The number of ZHe ages older than 400 Ma, if present, is indicated to the right of each diagram. Samples from the Upper Rhine Graben (P36) are displayed at the left-hand side, samples from the Lower Rhine Embayment are displayed on the right-hand side.

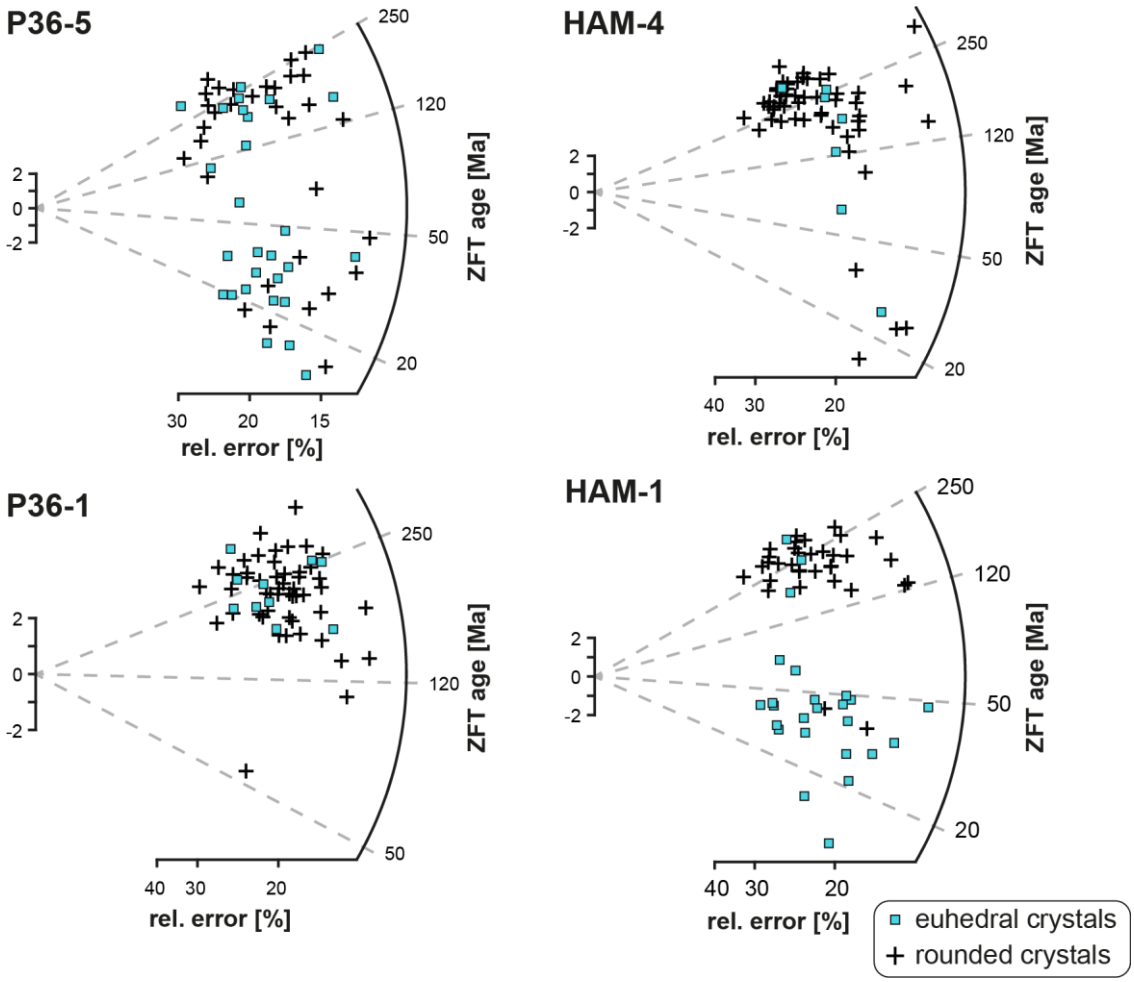

Figure 6: Radial plots showing zircon fission track ages and the morphology of the zircon grains (cross: rounded, square: euhedral). Remarkable is the dominance of euhedral crystals with Cenozoic ZFT ages in samples HAM-1 and P36-5.

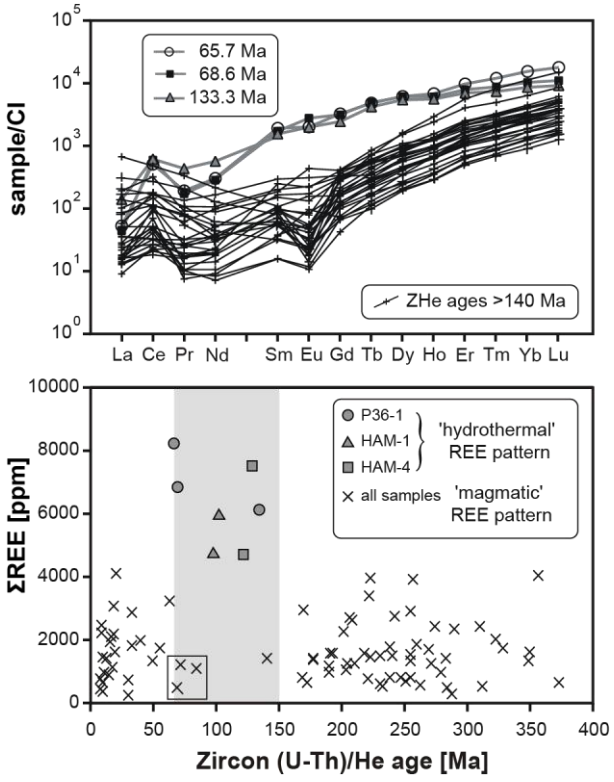

Figure 7: (a) Chondrite (CI) normalized (Anders & Grevesse, 1989) REE patterns of zircon grains from sample P36-1. Grains bearing the youngest (i.e. Cretaceous) ZHe ages show high total REE concentrations and higher abundances of the mid-REE compared to all other crystals, indicating hydrothermal formation or alteration (Hoskin, 2005). (b) ZHe age vs. total REE concentration of all dated zircon grains in which REE concentrations could be determined (n= 93). Samples with highest total REE concentrations exclusively occur in the age range from 150 to 65 Ma (grey bar) which corresponds to the time span of hydrothermal activity that affected the European crust (Wetzel et al., 2003; Romer et al., 2010). The box indicates three crystals with Late Cretaceous ZHe ages and low total REE content <1200 ppm from sample P36-5 (see text).

Table 2: Results from zircon (U-Th)/He single-grain thermochronology obtained on the selected samples from the Upper Rhine Graben and the Lower Rhine Embayment.

		He		U^{238}			Th^{232}				Eject.	*Uncorr.*	Ft-Corr.	
		vol.	1s	mass	1s	conc.	mass	1s	conc.	Th/U	corr.	*He-age*	He-age	2s
Sample	aliq.	[ncc]	[%]	[ng]	[%]	[ppm]	[ng]	[%]	[ppm]	ratio	(Ft)	*[Ma]*	[Ma]	[Ma]
DX-8, Keuper reference sample														
	#1	**32.24**	1.6	**1.54**	1.8	499	**0.62**	2.4	201	0.40	**0.74**	*155.8*	**210.4**	19.0
	#2	**35.16**	1.6	**1.53**	1.8	260	**1.19**	2.4	201	0.77	**0.78**	*158.6*	**203.3**	16.2
	#3	**6.64**	1.7	**0.32**	1.8	54	**0.36**	2.4	60	1.11	**0.78**	*134.6*	**172.2**	13.7
	#4	**43.51**	1.6	**2.05**	1.8	400	**1.40**	2.4	274	0.69	**0.74**	*149.5*	**201.9**	18.2
V-35, Rotliegend reference sample														
	#1	**38.94**	1.6	**1.16**	1.8	276	**0.49**	2.4	116	0.42	**0.75**	*246.6*	**328.9**	28.9
	#2	**36.63**	1.6	**0.92**	1.8	154	**1.04**	2.4	173	1.13	**0.79**	*254.7*	**323.9**	25.2
	#3	**15.97**	1.6	**0.37**	1.9	61	**0.84**	2.4	139	2.27	**0.78**	*228.1*	**293.9**	23.6
P36-1														
	#1	**36.22**	1.6	**1.72**	1.8	520	**0.14**	2.4	44	0.08	**0.76**	*168.8*	**222.2**	19.1
	#2	**28.20**	1.6	**4.33**	1.8	2370	**2.99**	2.4	1638	0.69	**0.67**	*46.2*	**68.6**	7.4
	#3	**48.31**	1.6	**1.92**	1.8	866	**0.28**	2.4	128	0.15	**0.74**	*198.3*	**268.6**	24.6
	#4	**24.49**	1.6	**0.74**	1.8	519	**0.31**	2.4	217	0.42	**0.74**	*243.9*	**328.2**	29.4
	#5	**23.85**	1.6	**0.82**	1.8	328	**0.58**	2.4	233	0.71	**0.77**	*202.5*	**262.5**	21.5
	#6	**18.68**	1.6	**0.97**	1.8	631	**0.57**	2.4	373	0.59	**0.73**	*138.4*	**190.8**	17.9
	#7	**45.07**	1.6	**1.68**	1.8	730	**0.86**	2.4	372	0.51	**0.75**	*194.9*	**259.0**	22.6
	#8	**59.78**	1.6	**2.13**	1.8	473	**0.48**	2.4	106	0.22	**0.77**	*217.1*	**282.3**	23.6
	#9	**86.79**	1.6	**3.62**	1.8	485	**0.58**	2.4	77	0.16	**0.79**	*188.2*	**238.5**	18.8
	#10	**17.67**	1.6	**0.74**	1.8	190	**0.27**	2.4	70	0.37	**0.78**	*178.6*	**229.9**	18.7
	#11	**72.29**	1.6	**2.82**	1.8	528	**0.92**	2.4	173	0.33	**0.76**	*194.0*	**254.2**	21.5
	#12	**29.60**	1.6	**1.23**	1.8	308	**0.37**	2.4	94	0.30	**0.77**	*183.8*	**240.1**	20.2
	#13	**43.08**	1.6	**1.88**	1.8	522	**1.90**	2.4	528	1.01	**0.74**	*151.4*	**204.1**	18.2
	#14	**92.57**	1.6	**2.99**	1.8	370	**1.23**	2.4	153	0.41	**0.81**	*229.3*	**283.3**	20.7
	#15	**14.72**	1.6	**0.27**	1.9	85	**0.14**	2.4	45	0.53	**0.74**	*395.0*	**531.0**	47.7
	#16	**73.84**	1.6	**2.99**	1.8	420	**1.22**	2.4	170	0.41	**0.80**	*183.5*	**230.1**	17.5
	#17	**17.16**	1.6	**0.51**	1.8	254	**0.12**	2.4	60	0.24	**0.70**	*259.4*	**372.5**	38.2
	#18	**13.63**	1.6	**0.41**	1.8	166	**0.22**	2.4	90	0.54	**0.72**	*237.0*	**331.0**	32.0
	#19	**5.75**	1.7	**0.12**	2.3	147	**0.09**	2.5	111	0.75	**0.44**	*326.7*	**750.0**	132.4
	#20	**28.75**	1.6	**2.12**	1.8	777	**0.31**	2.4	114	0.15	**0.76**	*107.4*	**140.5**	11.9
	#21	**42.67**	1.6	**1.89**	1.8	397	**0.95**	2.4	198	0.50	**0.78**	*164.5*	**209.7**	16.6
	#22	**35.89**	1.6	**1.63**	1.8	419	**0.71**	2.4	181	0.43	**0.79**	*162.7*	**206.0**	16.1
	#23	**60.13**	1.6	**1.67**	1.8	352	**0.40**	2.4	83	0.24	**0.79**	*274.9*	**349.5**	27.7
	#24	**144.58**	1.6	**8.81**	1.8	1595	**10.10**	2.4	1829	1.15	**0.80**	*106.0*	**133.3**	10.1
	#25	**33.32**	1.6	**1.57**	1.8	438	**0.17**	2.4	46	0.11	**0.77**	*168.9*	**220.8**	18.7
	#26	**52.21**	1.6	**8.13**	1.8	2848	**3.22**	2.4	1130	0.40	**0.74**	*48.4*	**65.7**	6.0
	#27	**45.71**	0.9	**1.51**	1.8	255	**0.72**	2.4	122	0.48	**0.79**	*221.0*	**278.8**	20.0
	#28	**39.77**	0.9	**1.52**	1.8	492	**0.38**	2.4	122	0.25	**0.73**	*200.6*	**274.0**	24.3
	#29	**10.24**	0.9	**0.44**	1.8	111	**0.20**	2.4	51	0.46	**0.76**	*173.2*	**227.8**	18.4
	#30	**30.46**	0.9	**1.06**	1.8	232	**0.40**	2.4	87	0.38	**0.76**	*215.2*	**283.1**	22.9
	#31	**21.53**	0.9	**0.78**	1.8	172	**0.05**	2.5	11	0.06	**0.78**	*221.6*	**285.1**	22.0
	#32	**17.20**	0.9	**0.93**	1.8	247	**0.21**	2.4	56	0.23	**0.76**	*143.2*	**187.8**	15.1
	#33	**49.10**	0.8	**1.75**	1.8	291	**0.63**	2.4	105	0.36	**0.79**	*210.5*	**267.8**	19.8

Table 2 cont.

		He		U^{238}			Th^{232}				Eject.	*Uncorr.*	Ft-Corr.	
Sample	aliq.	vol. [ncc]	1s [%]	mass [ng]	1s [%]	conc. [ppm]	mass [ng]	1s [%]	conc. [ppm]	Th/U ratio	Corr. (Ft)	*He-age [Ma]*	He-age [Ma]	2s [Ma]
P36-5														
	#1	**3.12**	1.7	**3.37**	1.8	469	**1.42**	2.4	198	0.42	**0.77**	*7.0*	**9.1**	0.8
	#2	**4.89**	1.7	**2.66**	1.8	598	**0.28**	2.4	62	0.10	**0.81**	*14.9*	**18.3**	1.3
	#3	**3.00**	1.7	**0.43**	1.8	123	**0.15**	2.4	44	0.36	**0.77**	*53.7*	**69.3**	5.7
	#4	**8.06**	1.6	**5.06**	1.8	901	**1.48**	2.4	264	0.29	**0.77**	*12.3*	**16.0**	1.3
	#5	**45.90**	1.6	**1.51**	1.8	444	**1.21**	2.4	354	0.80	**0.77**	*207.7*	**271.4**	22.6
	#6	**29.01**	1.6	**14.61**	1.8	2118	**2.83**	2.4	410	0.19	**0.79**	*15.7*	**19.9**	1.6
	#7	**1.07**	1.7	**1.28**	1.8	528	**0.16**	2.4	64	0.12	**0.73**	*6.7*	**9.3**	0.9
	#8	**22.42**	1.6	**6.24**	1.8	1926	**2.61**	2.4	805	0.42	**0.82**	*27.0*	**33.1**	2.4
	#9	**1.45**	1.7	**1.90**	1.8	705	**0.09**	2.4	35	0.05	**0.76**	*6.3*	**8.2**	0.7
	#10	**16.99**	1.6	**2.01**	1.8	580	**0.72**	2.4	209	0.36	**0.76**	*64.1*	**84.0**	7.1
	#11	**1.44**	1.7	**0.90**	1.8	317	**0.22**	2.4	78	0.25	**0.77**	*12.5*	**16.2**	1.3
	#12	**1.38**	1.7	**1.30**	1.8	187	**0.74**	2.4	106	0.57	**0.78**	*7.7*	**10.0**	0.8
	#13	**2.52**	1.7	**1.47**	1.8	364	**0.23**	2.4	58	0.16	**0.80**	*13.7*	**17.1**	1.3
	#14	**9.56**	1.6	**7.66**	1.8	3150	**0.40**	2.4	164	0.05	**0.84**	*10.2*	**12.2**	0.8
	#15	**2.10**	1.7	**1.30**	1.8	326	**0.43**	2.4	108	0.33	**0.86**	*12.4*	**14.4**	0.9
	#16	**69.66**	1.6	**2.29**	1.8	744	**2.24**	2.4	726	0.98	**0.85**	*201.2*	**237.8**	15.2
	#17	**12.57**	1.6	**3.59**	1.8	507	**1.26**	2.4	178	0.35	**0.81**	*26.7*	**33.0**	2.4
	#18	**32.10**	1.6	**7.51**	1.8	1024	**4.10**	2.4	560	0.55	**0.79**	*31.3*	**39.6**	3.1
	#19	**16.63**	0.8	**4.43**	1.8	530	**0.98**	2.4	118	0.22	**0.82**	*29.5*	**35.8**	2.3
	#20	**13.42**	0.8	**3.75**	1.8	718	**0.88**	2.4	168	0.23	**0.76**	*28.0*	**36.6**	2.9
	#21	**9.14**	1.7	**3.19**	1.8	955	**1.10**	2.4	330	0.35	**0.72**	*21.9*	**30.4**	2.9
	#22	**35.08**	0.8	**0.30**	1.9	88	**0.15**	2.4	45	0.51	**0.76**	*807.3*	**1058.5**	84.7
	#23	**45.70**	0.8	**1.33**	1.8	312	**0.62**	2.4	147	0.47	**0.78**	*251.4*	**321.2**	23.9
	#24	**7.46**	0.9	**2.29**	1.8	405	**1.59**	2.4	281	0.69	**0.81**	*23.1*	**28.6**	1.9
	#25	**59.72**	1.6	**3.76**	1.8	834	**0.27**	2.4	61	0.07	**0.76**	*127.8*	**168.2**	14.5
	#26	**34.59**	1.6	**1.67**	1.8	614	**0.46**	2.4	169	0.28	**0.78**	*159.1*	**203.4**	16.3
	#27	**8.34**	1.6	**11.67**	1.8	2112	**0.27**	2.4	48	0.02	**0.74**	*5.9*	**7.9**	0.7
	#28	**12.48**	1.6	**1.80**	1.8	434	**0.21**	2.4	50	0.12	**0.77**	*55.8*	**72.0**	5.9
	#29	**8.00**	1.6	**2.55**	1.8	300	**0.62**	2.4	73	0.24	**0.81**	*24.6*	**30.5**	2.3
	#30	**4.30**	1.7	**4.66**	1.8	1436	**0.07**	2.4	23	0.02	**0.77**	*7.6*	**9.9**	0.8
HAM-1														
	#1	**53.78**	1.6	**2.22**	1.8	261	**0.28**	2.4	33	0.13	**0.77**	*191.4*	**247.2**	20.4
	#2	**118.03**	1.6	**10.58**	1.8	1402	**6.84**	2.4	906	0.65	**0.82**	*79.6*	**97.2**	6.9
	#3	**21.20**	1.6	**1.13**	1.8	375	**0.94**	2.4	314	0.84	**0.73**	*128.6*	**177.4**	16.6
	#4	**40.46**	1.6	**1.97**	1.8	553	**0.68**	2.4	190	0.34	**0.77**	*155.0*	**201.8**	16.8
	#5	**81.11**	1.6	**7.47**	1.8	1652	**4.72**	2.4	1045	0.63	**0.76**	*77.7*	**101.7**	8.5
	#6	**100.20**	1.6	**4.25**	1.8	757	**1.51**	2.4	269	0.36	**0.80**	*177.4*	**221.4**	16.7
	#7	**34.45**	1.6	**1.29**	1.8	483	**0.44**	2.4	166	0.34	**0.73**	*201.2*	**273.8**	25.2
	#8	**18.33**	1.6	**0.91**	1.8	515	**0.65**	2.4	365	0.71	**0.73**	*140.9*	**192.2**	17.6
	#9	**56.44**	1.6	**1.91**	1.8	407	**0.76**	2.4	162	0.40	**0.86**	*219.0*	**254.9**	15.9
	#10	**48.42**	1.6	**1.81**	1.8	427	**0.16**	2.4	37	0.09	**0.74**	*212.9*	**287.6**	26.2
	#11	**44.57**	1.6	**1.69**	1.8	246	**1.44**	2.4	210	0.85	**0.74**	*178.7*	**242.3**	21.9
	#12	**53.16**	1.6	**0.84**	1.8	172	**0.36**	2.4	74	0.43	**0.71**	*457.9*	**648.1**	64.3
	#13	**23.49**	1.6	**1.17**	1.8	148	**0.36**	2.4	46	0.31	**0.81**	*153.2*	**189.9**	14.1
	#14	**28.39**	1.6	**0.71**	1.8	209	**0.29**	2.4	85	0.41	**0.68**	*294.1*	**430.8**	45.5
	#15	**9.96**	1.6	**0.57**	1.8	117	**0.38**	2.4	77	0.66	**0.72**	*123.8*	**172.4**	16.5
	#16	**38.58**	1.6	**1.23**	1.8	459	**0.36**	2.4	136	0.30	**0.74**	*238.6*	**322.1**	29.2
	#17	**2.52**	1.7	**0.10**	2.1	43	**0.07**	2.4	33	0.77	**0.71**	*178.7*	**250.4**	24.7
	#18	**2.80**	1.7	**0.78**	1.8	120	**1.07**	2.4	165	1.37	**0.75**	*22.3*	**29.8**	2.6
	#19	**0.64**	1.2	**0.11**	2.2	27	**0.12**	2.4	29	1.06	**0.77**	*38.4*	**50.0**	4.1
	#20	**5.79**	0.9	**1.26**	1.8	144	**2.50**	2.4	285	1.98	**0.79**	*25.8*	**32.5**	2.3
	#21	**2.57**	1.7	**1.10**	1.8	124	**1.21**	2.4	137	1.10	**0.79**	*15.4*	**19.5**	1.5
	#22	**35.30**	0.8	**1.22**	1.8	144	**0.42**	2.4	49	0.34	**0.80**	*216.8*	**271.9**	19.3
	#23	**65.60**	0.8	**2.19**	1.8	297	**0.54**	2.4	73	0.25	**0.80**	*229.4*	**286.8**	20.2
	#24	**71.28**	0.8	**1.91**	1.8	364	**1.02**	2.4	194	0.53	**0.79**	*267.8*	**337.7**	24.2

Table 2 cont.

		He		U^{238}			Th^{232}				Eject.	*Uncorr.*	Ft-Corr.	
Sample	aliq.	vol. [ncc]	1s [%]	mass [ng]	1s [%]	conc. [ppm]	mass [ng]	1s [%]	conc. [ppm]	Th/U ratio	corr. (Ft)	*He-age [Ma]*	He-age [Ma]	2s [Ma]
	#25	**17.67**	0.8	**0.47**	1.8	169	**0.05**	2.5	17	0.10	**0.73**	*294.7*	**401.1**	35.4
	#26	**40.95**	0.8	**1.30**	1.8	282	**0.19**	2.4	42	0.15	**0.78**	*245.9*	**314.1**	23.6
	#27	**31.66**	1.6	**1.21**	1.8	241	**0.41**	2.4	82	0.34	**0.77**	*196.9*	**256.2**	21.3
	#28	**9.05**	1.6	**0.37**	1.9	83	**0.37**	2.4	85	1.02	**0.75**	*162.6*	**217.4**	19.1
	#29	**77.38**	1.6	**2.68**	1.8	400	**0.22**	2.4	32	0.08	**0.80**	*230.2*	**289.3**	22.4
	#30	**44.53**	1.6	**1.50**	1.8	304	**0.19**	2.4	38	0.12	**0.75**	*233.3*	**309.3**	27.1
	#31	**23.07**	1.6	**1.17**	1.8	429	**0.31**	2.4	113	0.26	**0.73**	*151.3*	**208.3**	19.7
	#32	**28.29**	1.6	**1.08**	1.8	296	**0.60**	2.4	165	0.56	**0.74**	*188.7*	**254.5**	22.9
	#33	**4.10**	1.7	**0.13**	2.2	310	**0.02**	2.6	47	0.15	**0.45**	*253.4*	**562.3**	97.3
HAM-4														
	#1	**19.30**	1.6	**0.84**	1.8	193	**0.41**	2.4	93	0.48	**0.76**	*168.3*	**222.8**	19.3
	#2	**74.40**	1.6	**2.88**	1.8	533	**1.34**	2.4	247	0.46	**0.75**	*189.8*	**254.5**	22.6
	#3	**0.47**	5.0	**0.09**	18.7	1134	**0.02**	2.8	2588	0.23	**0.76**	*14.0*	**18.4**	3.2
	#4	**6.84**	1.6	**6.96**	1.8	1137	**2.56**	2.4	419	0.37	**0.76**	*7.5*	**9.9**	0.8
	#5	**20.79**	1.6	**1.23**	1.8	288	**0.48**	2.4	113	0.39	**0.71**	*126.6*	**177.4**	17.3
	#6	**24.43**	1.6	**0.78**	1.8	108	**0.31**	2.4	43	0.40	**0.75**	*233.0*	**311.2**	27.5
	#7	**20.17**	1.6	**0.82**	1.8	118	**0.31**	2.4	45	0.38	**0.79**	*184.9*	**232.8**	17.9
	#8	**2.72**	1.7	**2.70**	1.8	943	**0.28**	2.4	100	0.11	**0.77**	*8.1*	**10.5**	0.9
	#9	**32.03**	1.6	**0.53**	1.8	266	**0.15**	2.4	74	0.28	**0.73**	*453.2*	**621.7**	58.3
	#10	**71.12**	1.6	**4.47**	1.8	1247	**0.29**	2.4	80	0.06	**0.76**	*128.4*	**169.7**	14.8
	#11	**7.15**	1.7	**0.18**	2.0	47	**0.23**	2.4	60	1.29	**0.71**	*247.5*	**348.8**	34.3
	#12	**92.45**	1.6	**6.19**	1.8	1601	**2.40**	2.4	621	0.39	**0.79**	*112.2*	**142.9**	11.3
	#13	**48.16**	1.6	**1.45**	1.8	403	**1.10**	2.4	303	0.75	**0.71**	*228.4*	**319.9**	31.0
	#14	**18.23**	1.6	**0.44**	1.8	158	**0.29**	2.4	105	0.66	**0.74**	*290.4*	**392.3**	35.3
	#15	**17.19**	1.6	**0.60**	1.8	238	**0.32**	2.4	128	0.54	**0.74**	*208.3*	**282.3**	25.7
	#16	**19.90**	1.6	**0.70**	1.8	215	**0.69**	2.4	212	0.98	**0.76**	*187.2*	**246.7**	20.9
	#17	**6.72**	1.7	**0.27**	1.9	691	**0.22**	2.4	568	0.82	**0.72**	*172.0*	**238.0**	22.6
	#18	**82.79**	1.6	**6.74**	1.8	1430	**2.22**	2.4	471	0.33	**0.73**	*93.6*	**128.4**	12.0
	#19	**7.08**	1.6	**0.17**	2.1	55	**0.19**	2.4	59	1.08	**0.73**	*260.3*	**356.0**	33.2
	#20	**1.19**	1.7	**0.21**	2.0	6083	**0.05**	2.5	1575	0.26	**0.78**	*43.1*	**55.1**	4.5
	#21	**15.52**	1.6	**3.34**	1.8	491	**0.84**	2.4	124	0.25	**0.74**	*36.3*	**49.3**	4.5
	#22	**12.72**	1.6	**0.64**	1.8	172	**0.32**	2.4	87	0.50	**0.76**	*145.1*	**189.7**	15.9
	#23	**0.49**	1.8	**0.07**	2.8	4592	**0.04**	2.6	2506	0.55	**0.78**	*49.1*	**63.1**	5.6
	#24	**2.81**	1.7	**0.20**	2.0	9885	**0.15**	2.4	7242	0.73	**0.78**	*93.9*	**120.8**	9.8
	#25	**25.20**	0.9	**0.85**	1.8	166	**0.21**	2.4	41	0.24	**0.78**	*227.3*	**290.2**	21.7
	#26	**97.77**	0.8	**1.57**	1.8	322	**0.93**	2.4	192	0.60	**0.77**	*436.2*	**566.3**	43.9
	#27	**1.07**	1.0	**1.10**	1.8	289	**0.18**	2.4	48	0.17	**0.76**	*7.8*	**10.2**	0.8
	#28	**32.70**	0.8	**1.22**	1.8	327	**0.42**	2.4	113	0.34	**0.76**	*202.4*	**267.1**	21.7
	#29	**22.37**	0.9	**1.00**	1.8	314	**0.61**	2.4	191	0.61	**0.73**	*160.0*	**218.8**	19.3
	#30	**40.42**	0.9	**1.41**	1.8	326	**0.56**	2.4	130	0.40	**0.77**	*213.5*	**279.0**	22.1
	#31	**53.60**	0.9	**1.66**	1.8	281	**0.99**	2.4	167	0.59	**0.78**	*229.6*	**293.6**	21.8

Table 3: Results from zircon fission track thermochronology.

Sample	Cryst.	Spontaneous	Induced	Dosimeter	$P(\chi^2)$	Disp.	ZFT central age
		r_s (N_s)	r_i (N_i)	r_d (N_d)	[%]		[Ma ± 1s]
P36-5	60	102 (6309)	59.5 (3682)	7.30 (3214)	0	0.96	74 ± 9
P36-1	60	180 (9385)	36.5 (1904)	7.15 (3214)	0	0.27	219 ± 11
HAM-4	60	141 (7740)	34.9 (1920)	7.05 (3214)	0	0.89	177 ± 21
HAM-1	60	78 (5539)	32.7 (2323)	7.25 (3214)	0	0.91	96 ± 12

Cryst: number of dated zircon crystals.

Track densities (r) are as measured (x10^5 tr/cm^2); number of tracks counted (N) shown in brackets.

$P(c^2)$: probability obtaining Chi-square value for n degree of freedom (where n= no. crystals-1).

Disp.: Dispersion, according to Galbraith and Laslett (1993).

Central ages calculated using dosimeter glass CN 2 with ζ_{CN2} = 127.8 ± 1.6 (1 S.E.).

Table 4: Major age components in ZHe and ZFT single-grain data isolated using 'PopShare' (Dunkl & Székely, 2002).

			Alpine-derived (except for **) age components [Ma]			**not indicative (in traces)** [Ma]	**Mainly European-derived** age components [Ma]	
URG	**P36-5**	**ZHe**	9 ± 1 (25%)	16 ± 2 (20%)	32 ± 4 (28%)*	71 ± 3 (10%)		219 ± 59 (17%)
	(L. Pleistocene)	**ZFT**		17 ± 4 (14%)	32 ± 8 (19%)			203 ± 67 (59%)
	P36-1	**ZHe**				~67 (6%)	137 (6%)	250 ± 47 (88%)
	(Pliocene)	**ZFT**				~56 (<2%)		235 ± 59 (98%)
LRE	**HAM-4**	**ZHe**	10 ± 1 (14%)		58 ± 5 (10%)			253 ± 67 (76%)
	(L. Pleistocene)	**ZFT**		27 ± 12 (11%)				262 ± 85 (89%)
	HAM-1	**ZHe**		28 ± 11 (14%)**		99 ± 5 (9%)		250 ± 50 (77%)
	(Pliocene)	**ZFT**		30 ± 10 (7%) **	42 ± 5 (25%)	~70 (~7%)		230 ± 76 (62%)

* cooling ages, as demonstrated by the pre-Mesozoic U/Pb ages

** Central European volcanism, as demonstrated by the Oligocene U/Pb ages

Discussion

Linking sediment characteristics to potential sources

The combined application of a range of geochemical and geochronological methods to detrital zircons together with heavy mineral analyses allows placing relatively tight constraints on sediment sources. We demonstrate this case for Pliocene and Pleistocene Palaeo-Rhine sediment of the URG and the LRE. Sediment sources are identified by means of ZHe- and ZFT age distributions and distinct age

components. Zircon REE patterns, heavy mineral composition, and (for the Pleistocene URG sample and the Pliocene LRE sample) zircon U/Pb ages eradicate remaining ambiguity in source allocation.

Pliocene Upper Rhine Graben sediment (P36-1)

The ZHe (n= 33) and ZFT (n= 60) age spectra of the Upper Pliocene sample from the URG (P36-1) are strongly dominated by Variscan to Mesozoic ages (Fig. 5). The predominance of Permian to Jurassic ages implies that the Pliocene Palaeo-Rhine almost exclusively drained source areas belonging to the Central European platform. Besides Variscan crystalline basement, the units potentially delivering such zircons are clastic sediments from the Triassic Buntsandstein and Keuper (Fig. 2b and section 'Synopsis of low-temperature thermochronological data from the Rhine catchment'). This interpretation is corroborated by a dominantly stable heavy mineral assemblage (Fig. 3).

The lack of Cenozoic cooling ages that are characteristic for the Alps and the NAFB (Fig. 2b and section 'Synopsis of low-temperature thermochronological data from the Rhine catchment') suggests that no material from the Alps or the NAFB reached the URG at the time of deposition of sample P36-1 (i.e. 3.2-3.0 Ma, Piacenzian, Late Pliocene). This conclusion is based on low temperature thermochronological information from 93 detrital zircons. In statistical terms, any fraction of zircons >5% that has experienced thermal overprint exceeding the ZFT closure temperature can be excluded with 95% certainty (assuming non-uniform 'average' population according to Vermeesch, 2004). A small fraction of zircons from sample P36-1 bears Early to Late Cretaceous ZHe or ZFT ages (Fig. 5). In case of ZHe, four of 33 grains are dated at 66, 69, 133 and 141 Ma (Table 2). Although Cretaceous zircon cooling ages are reported from the Alps and the NAFB (Spiegel et al., 2000; Miller, 2012), this option is highly unlikely as discussed below. Central European basement outcrops that experienced Late Cretaceous exhumation and cooling are potential sources for such zircon grains as demonstrated for regions n the northeast of the Rhine catchment (Fischer et al., 2012). Variscan basement exposures close to the URG (e.g. Vosges, Black Forest) might also deliver zircons with Cretaceous ZHe cooling ages because the Mesozoic (hydro-) thermal pulse caused an overall reset of the AFT thermochronometer in the Cretaceous and even affected ZFT ages (Timar-Geng et al., 2006). From the southern Black Forest, Dresmann et al. (2010) reported Cretaceous single-grain ZFT ages as young as 109 Ma. These cooling ages were detected in the vicinity of ore districts that are densely penetrated by hydrothermal veins. Hydrothermally grown or hydrothermally influenced zircon crystals differ from those of magmatic zircon in terms of their REE pattern (Hoskin, 2005). Therefore, trace element analyses (32 elements) were performed on all (U-Th)/He dated zircon crystals and REE signatures of individual zircons were linked to ZHe cooling ages. The three youngest (Cretaceous) ZHe ages in sample P36-1 are characterized by considerably higher total REE concentrations, especially in the mid-REE range, leading to overall flatter mid- to heavy REE patterns compared to the rest of the single-grain ages >140 Ma (Fig. 7a). These features are characteristic for hydrothermally influenced zircon crystals that typically occur in the vicinity of ore deposits (Hoskin, 2005). Therefore, the few crystals with Cretaceous ZHe ages in sample P36-1 were hydrothermally influenced and most likely derived from the mineralized zones of the Black Forest or Vosges basement in

the southern URG. This interpretation is supported by the relation between total REE concentrations and ZHe ages which reveals that hydrothermal zircons (as characterized above) are restricted to Late Jurassic to Late Cretaceous ages (ca. 150-65 Ma), i.e. between the main Cenozoic ('Alpine') and Variscan to Jurassic ('European') age clusters, which both show lower total REE concentrations (Fig. 7b).

Contrary to our observations, detrital AFT analyses from Pliocene Rhine sediments (Reiter et al., 2013) have been interpreted to record sediment transport from the northern margin of the Alps (i.e. Subalpine Molasse, NAFB) to the Pliocene URG already at ~3.6 Ma. This interpretation is built on a 'poorly defined' age group around 18 Ma, which is based on very few apatite grains (i.e. 17.5 ± 9.2 Ma, n= 3; 19.4 ± 16.0 Ma, n= 2; Reiter et al., 2013; Tables 1 and 2). A possible origin of these grains from the coeval Kaiserstuhl volcanism has been 'largely ruled out' by these authors due to grain morphology and small D-par values. However, for two main reasons we think that sources in the Kaiserstuhl with Miocene AFT cooling ages can not be ruled out. First, diverse geologic evidence suggests that the Middle to Late Pliocene southern drainage divide of the river Rhine was located close to the Kaiserstuhl area (Villinger, 2003; Berger et al., 2005; Ziegler & Fraefel, 2009). The highly weathered and deeply eroded Kaiserstuhl alkaline volcanic complex constitutes a prominent geomorphic and geologic feature in the southern URG and contains a variety of apatite-bearing volcanic rocks. Second, the Kaiserstuhl volcanism has thermally affected Tertiary sediments (Groschopf et al., 1996; Wimmenauer, 2003) and might hence yield rounded apatite with Miocene cooling ages. Three facts suggest that there was no connection of the URG drainage system to the Alps or NAFB before the Late Piacenzian (i.e. before ca. 3.0 Ma): (i) the debatable origin of minor apatite with Miocene FT cooling age in ~3.6 to ~3.2 Ma old Pliocene strata as outlined above, (ii) the comparatively strong and statistically significant evidence for the lack of Alpine material in the URG until at least ~3.2 to ~3.0 Ma from our new zircon thermochronological data, and (iii) various heavy mineral evidence that points to the onset of Alpine contribution to Rhine sediment in the latest Pliocene or at the Pliocene-Pleistocene boundary. The connection to the Alpine drainage system was fully established at the Pliocene-Pleistocene boundary (2.59 Ma).

Pleistocene Upper Rhine Graben sediment (P36-5)

The Early Pleistocene sample (P36-5) from the URG shows ZHe and ZFT age spectra that differ significantly from those of the Pliocene sediments from the same core (Figs 5 and 8). Very pronounced Cenozoic age components appear both in the ZHe and in the ZFT age distributions and clearly indicate Alpine provenance as well as a fully established connection of the URG to the Alpine drainage system. The NAFB and the Central Alps are the only sources in the catchment of the river Rhine that bear zircons with such young ages (Fig. 2b). The slightly older ZFT ages compared to ZHe ages arise from the higher closure temperature of the ZFT thermochronometer (Fig. 5). Cenozoic ZHe ages are characterized by a roughly bimodal age distribution comprising Miocene ages from 7.9 to 19.9 Ma (13 out of 21 grains) and Late Eocene to Oligocene ages from 28.6 to 39.6 Ma (Fig. 8, Table 2).

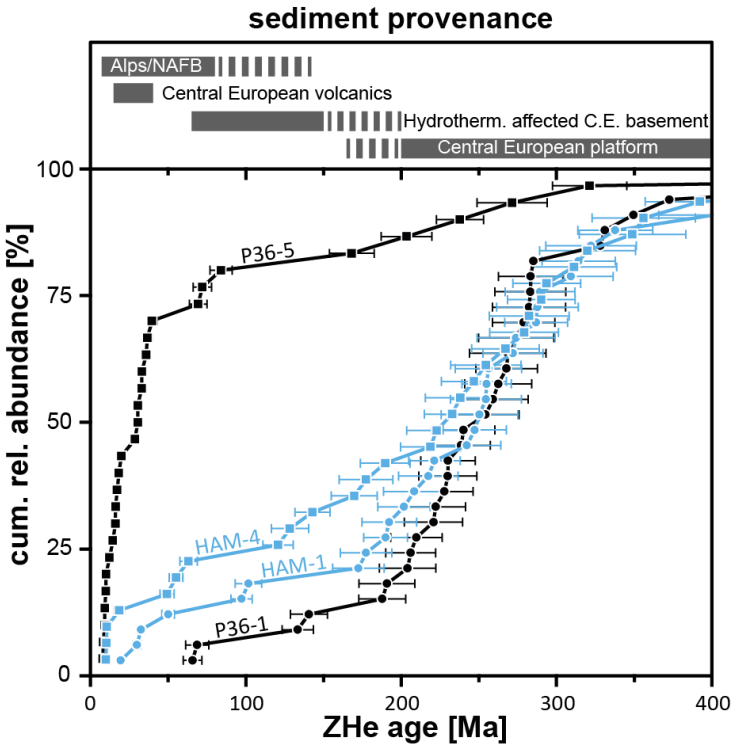

Figure 8: Cumulative ZHe age distributions of Pliocene (HAM- 1) and Pleistocene (HAM-4) Rhine sediments from the open cast mine Hambach in the Lower Rhine Embayment (LRE, blue symbols) and drill core P36 from the northern Upper Rhine Graben (URG, black symbols). Circles and squares indicate Pliocene and Pleistocene sediment samples respectively. The shift towards younger ZHe ages, especially from Pliocene to Lower Pleistocene URG samples (P36-1 to P36-5 respectively), represents a change in sediment provenance. Admixture of sediment derived from downstream sources that have older cooling ages is expressed in a shift towards lower numbers of crystals with Cenozoic ZHe ages (i.e. the Pleistocene LRE sample HAM-4 vs. the Pleistocene URG sample P36-5). CE, Central European.

The Miocene group shows two individual age components at 9 and 16 Ma (Table 4, Fig. 5), which are well-known from Central Alpine bedrock and modern rivers that drain the Aar- and Gotthard Massifs and the Lepontine Dome (Hurford, 1986; Bernet et al., 2004; Vernon et al., 2008; Fig. 6b). The older Cenozoic age component at 32 Ma (Table 4, Fig. 5) is roughly coeval to the Periadriatic volcanism (Brügel et al., 2000; Benedek et al., 2001; Dunkl et al., 2001). Four crystals, which form a tight age group between 33.1 and 30.4 Ma all have yellow to brownish colours and euhedral shapes. Zircon U/Pb geochronology performed on 55 euhedral zircon crystals from sample P36-5 yield Permo-Carboniferous and older U/Pb ages (Fig. 9), similar to the results from Middle Pleistocene Rhine sediments reported by Krippner & Bahlburg (2013). Periadriatic volcanic rocks must hence be excluded as potential source rocks. Therefore, yellow to brownish, euhedral zircon crystals in the Pleistocene URG sediments likely derive from Variscan granitoids and orthogneisses that experienced Oligocene thermal reset close the Periadtiatic intrusions or cooled from Barrovian metamorphic conditions in the Oligocene (Berger et al., 2011). Three zircon grains (Table 2) yield Late Cretaceous ZHe ages, which form a small age component at ~71 Ma (Table 4, Fig. 5). Their total REE concentration is below 1200 ppm, indicating the common 'magmatic' type zircon (Fig. 7b). Thus they most likely derive from Alpine bedrock with typical Late Cretaceous zircon cooling ages (Spiegel et al., 2000). Subordinate occurrences of Late Carboniferous to Jurassic ZHe ages either reflect sources in less uplifted and eroded regions in the Alps and/or the NAFB,

or contribution from tributaries draining the Black Forest and Vosges basement rocks and adjacent Mesozoic cover rocks (Fig. 2b). The latter option is considered less likely given the extremely high heavy mineral content of this sample (13.7 wt%; Fig. 2). Pliocene and Pleistocene sediments from the Lower Rhine Embayment (HAM-1 and HAM-4) In contrast to the URG, Late Pliocene (HAM-1) and Early Pleistocene (HAM-4) samples from the LRE do not show striking differences in their ZHe and ZFT age distributions (Figs 5 and 8, Table 4). This observation is at first glance surprising, given previous models of pronounced provenance shifts that are inferred from strong contrasts in heavy mineral composition across the Pliocene-Pleistocene boundary (Boenigk, 1978a; Boenigk & Frechen, 2006; Kemna, 2008a,b). This strong contrast in heavy mineral composition is also observed in our samples (Figs 3 and 4): the Pliocene sample reveals the typical European platform signature with a high proportion of ultra-stable heavy minerals (zircon, tourmaline, and TiO_2-phases; like the Pliocene sample of the URG), whereas the Pleistocene sample is characterized by a typical Alpine heavy mineral assemblage dominated by zoisite, epidote, amphibole, and garnet.

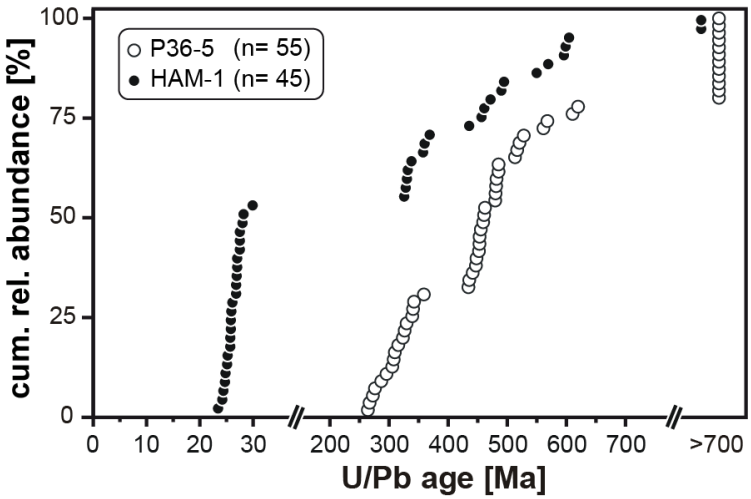

Figure 9: Cumulative relative abundance of zircon U/Pb ages of selected, euhedral, transparent crystals. The Precambrian ages are highly diffuse and do not form distinct age components.

The majority of zircon crystals in both samples (62-89%; Table 4) yields ZFT and ZHe ages between the Late Palaeozoic and Jurassic (Fig. 5). Although such cooling ages are present in Alpine bedrocks and in theNAFB (Spiegel et al., 2000), their contribution must be considered of minor importance (Bernet et al., 2004; Vernon et al., 2008, see section 'Synopsis of low-temperature thermochronological data from the Rhine catchment'). Consequently, the high proportion of Late Palaeozoic to Jurassic cooling ages, present in both Pliocene and Pleistocene sediments of the LRE, implies that the Alps cannot be a major source. Instead, this broad age component dominantly represents sources in the European basement and its cover rocks (see section 'Synopsis of low-temperature thermochronological data from the Rhine catchment'). Interestingly, the cumulative ZHe age distributions between 400 and 170 Ma are identical (within analytical uncertainty) in the Pliocene samples from URG and LRE (Fig. 8), supporting the interpretation of largely similar sources for zircons of the Late Palaeozoic to Jurassic age group in the Pliocene URG and LRE. This implication from

thermochronological data is evident but conflicts with implications from the heavy mineral compositions. While the latter conform to the established model of sediment provenance change, thermochronological data appears to disprove this scenario. We think that Rhine sediment develops such ambivalent character as it traverses the Rhenish Massif. There, mature (heavy mineral poor, but relatively zircon-rich) sediment is being admixed to immature (heavy mineral rich but relatively zircon-poor) sediment generated in the Alps. This example illustrates that provenance proxies based on single minerals and/or methods do not necessarily represent a robust record of sediment provenance. Thermochronological data alone might yield wrong conclusions.

Cenozoic ZHe and ZFT age components of both Pliocene and Pleistocene LRE samples range in proportion from 11% to 32% (Table 4). At first glance, this finding suggests Alpine contribution to the LRE already in the Late Pliocene (sample HAM-1). This component is relatively small (14%) in the ZHe data set but comprises about one-third of the crystals in the ZFT data set. Crystals belonging to this age component are almost exclusively euhedral (Fig. 6), and peak in Mid-Eocene to Oligocene time (Fig. 5). Interestingly, while nearly all other zircons with Cenozoic ZHe ages have Th/U ratios <0.7, the crystals with Cenozoic ZHe ages from the Pliocene LRE have high Th/U ratios >1.0 (Fig. 10). Values for Th/U that exceed 0.1-0.2 are generally considered typical for igneous zircon, however, high values of Th/U > 1.0 are uncommon for most igneous zircons (Hoskin & Ireland, 2000). This observation makes a common source of the young ZHe ages from Pleistocene (i.e. Alpine-derived; see above) and Pliocene sediment unlikely and thus, calls for a specific and not yet considered source for the zircons with Cenozoic low temperature cooling ages in Pliocene LRE sediment. We therefore dated selected euhedral zircons from sample HAM-1 by U/Pb. Besides Variscan and older ages, a distinct and significant Cenozoic age component dominates this sample (24 of 45 grains; Fig. 9). This age component ranges from 23.4 to 29.9 Ma with a mean age of 26.2 ± 0.3 Ma.

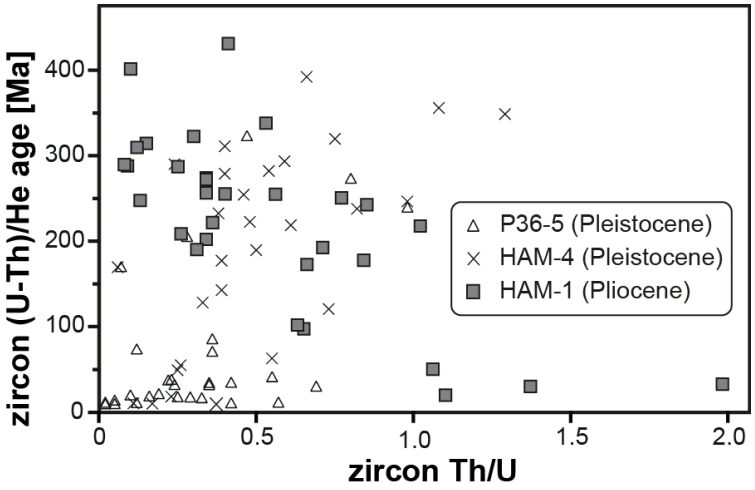

Figure 10: Relation between single-grain zircon (U-Th)/He ages and the ratio of actinide elements. Zircons with Cenozoic cooling ages are characterized by low (<0.7) Th/U ratios in the Pleistocene samples, while zircon Th/U ratios are >1 in the Pliocene sample.

Cenozoic volcanics in Central Europe, although volumetrically limited, might constitute an alternative source for the zircons with Oligocene crystallization- and cooling ages. Volcanic rocks from

the Tertiary alkaline intraplate volcanism cover significant areas around the Rhenish triple junction (Sissingh, 2003) with major occurrences in the Eifel, the Siebengebirge, the Vogelsberg massif and the Westerwald (Figs 1 and 2). Remarkably, these areas are drained by the lower reaches of the (Palaeo-)Rhine and its tributaries (e.g. Lahn, Mosel, Main) towards the LRE, but have not influenced deposits in the URG south of the triple junction (i.e. south of the Mainz Basin, e.g. borehole P36; Fig. 1). The main mass of the volcanic rocks is composed of alkali basalts and basanites. However, more differentiated rocks that might provide zircons like trachytes and latites occur as well (Wedepohl et al., 1994; Bogaard & Wörner, 2003; Haase et al., 2004; Feriakova et al., 2007a; Kolb et al., 2012). K/Ar whole-rock ages of the Tertiary volcanics mainly range from Eocene to Miocene with significant spatial variation (Lippolt, 1983), as confirmed by more recent Ar/Ar ages (Bogaard & Wörner, 2003; Feriakova et al., 2007b; Linthout et al., 2009). According to these data, Tertiary volcanism culminated at 44-35 Ma in the Eifel, at 30 to ~20 Ma in the Siebengebirge and Westerwald, and at 18-14 Ma in the Vogelsberg. From the Vogelsberg area, felsic volcanics yield latest Cretaceous (Schmitt et al., 2007; Martha et al., 2014) and Late Oligocene zircon U/Pb ages (26.2 Ma; Neuhaus, 2010). The latter age was determined on euhedral zircons from a trachytic tuff with elevated Th/U ratios of up to 1.8 (Axel Gerdes, Wolfgang Dörr; pers. comm., 2014). Thus, geochemical and geochronological characteristics of Central European volcanics are consistent with those of the euhedral Cenozoic zircon grains from Pliocene sediments of the LRE. Oligocene trachytic rocks are also exposed in the Westerwald and the Siebengebirge and are located even closer to the LRE. Trachytes and latites from the Siebengebirge (Drachenfels) directly adjacent to the Rhine valley have been dated at 27-25 Ma (Ar/Ar sanidine, Jan R. Wijbrans, pers. comm.; see also Kolb et al., 2012). We thus conclude that the felsic members of the Central European Cenozoic volcanic rocks, especially from the Vogelsberg, Westerwald, and Siebengebirge volcanic centres constitute the most likely source of the Oligocene zircons in Pliocene LRE sediments.

In the Pleistocene sample (HAM-4) the tight ZHe age component around 10 Ma (Table 4) closely matches the youngest ages observed in the Pleistocene URG sample (P36-5; Fig. 8), suggesting sources in the Aar- and Gotthard Massifs and/or the Lepontine Dome in the Central Alps (see section 'Synopsis of low-temperature thermochronological data from the Rhine catchment'). These zircons are too young to derive from the Central European Cenozoic volcanics. The second Cenozoic ZHe age component around 58 Ma (Table 4) resembles Early Tertiary age components reported from the Alps and the NAFB (Fig. 2B). Five grains with Cretaceous cooling ages are also present in both LRE samples, four of which have anomalously high REE contents and most likely represent contribution from the hydrothermally affected European basement (see above). The age components observed in the Pleistocene LRE thus largely resemble those of the Pleistocene URG, although proportions are different.

The presence of a much higher quantity of Palaeozoic and Mesozoic cooling ages in the Lower Pleistocene LRE sample (HAM-4) compared to the Lower Pleistocene URG sample (P36-5) along with a roughly similar Alpine-type heavy mineral assemblage can be readily explained by significant downstream admixture of material derived from the Central European platform. On a route of more than 120 km, the Rhine River crosses Late Palaeozoic metasedimentary rocks that are exposed in the Rhenish

Massif and gains sediment input from several tributaries restricted to the Central European platform such as rivers Mosel and Lahn (Figs 1 and 2a). This mixing phenomenon is not reflected in the heavy mineral spectra because the platform-derived sediment is characterized by low heavy mineral contents but relatively high zircon yields (Fig. 3). Comparable downstream dilution of Alpine signals has been described for modern Rhine sediment by Bernet et al. (2004). Admixture of zircon-rich but overall heavy mineral poor sediment could also have occurred close to the site of deposition, where local streams deliver extremely mature sediment, as represented by the Hambach beds (HAM-5; Figs 3 and 4). These deposits were found to be partially intercalated with Rhine deposits (Kemna, 2008b) and are therefore another straightforward explanation for the dominance of zircons with Central European provenance in sediments with typical immature, Alpine-type heavy mineral spectra (HAM-4, HAM-6).

Summary and conclusions

The combined application of several analytical methods including heavy mineral analysis, detrital zircon thermochronology (ZHe and ZFT) together with REE geochemistry and complementary zircon U/Pb analysis in the framework of the regional example of the river Rhine catchment allows to (i) explore ZHe dating as provenance proxy and further exploit its potential by single grain REE signatures that are gained as by-product of ZHe dating, (ii) demonstrate the advantages of method combination for provenance studies by revealing effects of sediment mixing on the provenance record, and (iii) provide new constraints on sediment sources of the (Palaeo-) Rhine that yield implications about the fluvial history of the Rhine River. We draw the following conclusions:

(1) The integration of ZFT and ZHe techniques adds the respective advantages of each method, which include higher number of single-grain ages (from ZFT) and higher single-grain age precision as well as additional geochemical data (from ZHe).

(2) Detrital ZHe and ZFT age spectra of samples from the URG corroborate results from previous work on heavy mineral composition of Rhine sediments, and suggest a large extension of the catchment area of the river Rhine that occurred in the latest Pliocene between ~3.0 and 2.59 Ma. The determination of 30- 33 single-grain ZHe ages and 60 ZFT ages per sample reveal a significant shift from mostly Permo-Mesozoic cooling ages in Upper Pliocene Rhine sediments towards dominantly Cenozoic cooling ages in Lower Pleistocene sediments, coinciding with a shift from ultra-stable heavy minerals to less stable heavy mineral assemblages.

(3) Pre-Cenozoic ZHe and ZFT ages are widely distributed between the Permian and the Cretaceous in both the Pliocene and the Pleistocene samples. This age distribution is representative of the Central European basement and its siliciclastic cover sequences that have been affected by long-lasting burial, hydrothermal-and exhumation processes.

(4) Cenozoic ZHe and ZFT cooling ages in Pleistocene URG sediments are derived from the Alps. A significant population of Late Miocene ZHe ages (9 ± 1 Ma) indicates sources in the Aar- and Gotthard Massifs and the Lepontine Dome. Further typical Alpine bedrock cooling ages are present as well-defined age components of 16 ± 2 Ma (ZHe), 17 ± 4 Ma (ZFT), 32 ± 4 Ma (ZHe) and 32 ± 8 Ma (ZFT) and unequivocally confirm Central Alpine origin. Especially the Oligocene age component might also represent recycled material derived from the North Alpine Foreland Basin.

(5) Pliocene sediments from the LRE (HAM-1) contain significant amounts of Cenozoic cooling ages. Th/U ratios and U/Pb ages reveal sources in Oligocene trachytic members of the Central European volcanism, most likely from the Vogelsberg, Westerwald or Siebengebirge volcanic centres and preclude Alpine sources.

(6) Relatively large proportions of Permo-Mesozoic zircon cooling ages in Alpine-type heavy mineral assemblages of Pleistocene sediments from the LRE demonstrate the sensitivity of sediment provenance proxies to sediment admixture.

(7) The combination of ZHe ages and REE signatures yields additional constraints on sediment provenance, especially when the age information alone is ambiguous with respect to source area discrimination. In case of the present example of Rhine sediments we show that zircons with Cretaceous cooling ages have characteristically high REE contents, flat REE patterns and can be assigned to hydrothermally influenced basement rocks exposed along the URG margins.

Acknowledgements

We thank Dr. Michael Weidenfeller (Landesamt für Geologie und Bergbau, Mainz) for permission and personal advice to sample drill core P36 from Ludwigshafen. We are grateful to Mr. Steinhauer, Mr. Göllner and Mr. Bauendahl (RWE AG) who made sampling in the open cast mine Hambach possible. Many thanks to Dr. Hans- Axel Kemna for guiding us through the Plio-Pleistocene stratigraphy of the lignite mine Hambach. We received the Rotliegend and Carnian samples from Veit-Enno Hoffmann and Josef Paul respectively. Many thanks for their valuable help. We greatly appreciate editorial handling by Peter van der Beek and Andreas Mulch. The paper benefitted from thorough and detailed reviews by Matthias Bernet, Wolfgang Reiter, Pieter Vermeesch, Christoph Glotzbach and Peter van der Beek.

References

ANDERS, E. & GREVESSE, N. (1989) Abundances of the elements: Meteoritic and solar. *Geochim. et Cosmochim. Acta*, 53, 197-214.

BENEDEK, K., NAGY, Z. R., DUNKL, I., SZABÓ, C. & JÓZSA, S. (2001) Petrographical, geochemical and geochronological constraints on igneous clasts and sediments hosted in the Oligo-Miocene Bakony Molasse, Hungary: Evidence for Paleo-Drava River system. *Int. J. Earth Sci.*, 90, 519-533.

BERGER, J.-P., REICHENBACHER B., BECKER, D., GRIMM, M., GRIMM, K., PICOT, L., STORNI, A., PIRKENSEER, C., DERER, C., & SCHAEFER, A. (2005) Paleogeography of the Upper Rhine Graben (URG) and the Swiss Molasse Basin (SMB) from Eocene to Pliocene. *Int. J. Earth Sci.*, 94, 697-710.

BERGER, A., SCHMID, S. M., ENGI, M., BOUSQUET, R. & WIEDERKEHR, M. (2011) Mechanisms of mass and heat transport during Barrovian metamorphism: A discussion based on field evidence from the Central Alps (Switzerland/northern Italy). *Tectonics*, 30, TC1007, doi:10.1029/2009TC002622.

BERNET, M., BRANDON, M.T., GARVER, J.I. & MOLITOR, B. (2004) Downstream Changes of Alpine Zircon Fission-Track Ages in the Rhone and Rhine Rivers: *Journal of Sedimentary Research*, 74 82-94.

BOENIGK, W. (1976) Schwermineraluntersuchungen zur Entwicklung des Rheinsystems: *Eiszeitalter und Gegenwart*, 27, 202.

BOENIGK, W. (1978a) Die flußgeschichtliche Entwicklung der Niederrheinischen Bucht im Jungtertiär und Altquartär. *Eiszeitalter und Gegenwart*, 28 1-9.

BOENIGK, W. (1978b) Gliederung der altquartären Ablagerungen in der Niederrheinischen Bucht. *Fortschritte in der Geologie von Rheinland und Westfalen*, 28, 135-212.

BOENIGK, W. & FRECHEN, M. (2006) The Pliocene and Quaternary fluvial archives of the Rhine system. *Quaternary Science Reviews*, 25, 550-574.

BOGAARD, P. & WÖRNER, G. (2003) Petrogenesis of Basanitic to Tholeiitic Volcanic Rocks from the Miocene Vogelsberg, Central Germany. *Journal of Petrology*, 44, 569-602.

BRÜGEL, A. DUNKL, I., FRISCH, W., KUHLEMANN, J. & BALOGH, K (2000) The record of Periadriatic volcanism in the Eastern Alpine Molasse zone and its paleogeographic implications. *Terra Nova*, 12, 42-47.

BRÜGEL, A., DUNKL, I., FRISCH, W., KUHLEMANN, J. & BALOGH, K. (2003) Geochemistry and geochronology of gneiss pebbles from foreland molasse conglomerates: geodynamic and paleogeographic implications for the Oligo-Miocene evolution of the Eastern Alps. *Journal of Geology*, 111, 543-563.

BURKHARD, M. (1990) Aspects of the large-scale Miocene deformation in the most external part of the Swiss Alps (Subalpine Molasse to Jura fold belt): *Eclogae Geologicae Helvetiae*, 83, 559-583.

CARTER, A. (2007) Heavy minerals and detrital fission-track thermochronology. In: *Developments in Sedimentology*, 58, 851-868.

CHERNIAK D.J. & WATSON E.B. (2001) Pb Diffusion in zircon. *Chemical Geology*, 172, 5-24.

DÈZES, P., SCHMID, S. M. & ZIEGLER, P. A. (2004) Evolution of the European Cenozoic Rift System: interaction of the Alpine and Pyrenean orogens with their foreland lithosphere. *Tectonophysics*, 389, 1-33.

DOORNENBAL, H. & STEVENSON, A. (2010) Petroleum Geological Atlas of the Southern Permian Basin Area, *EAGE Publications*, 352.

DRESMANN, H., KEULEN, N., TIMAR-GENG, Z., FÜGENSCHUH, B., WETZEL, A. & STÜNITZ, H. (2010) The south-western Black Forest and the Upper Rhine Graben Main Border Fault: thermal history and hydrothermal fluid flow. *Int. J. Earth Sci.*,99, 285-297.

DUMITRU, T. A. (1993) A new computer-automated microscope stage system for fission-track analysis. *Nucl. Tracks Radiat. Meas.* 21. 575-580.

DUNKL, I., DI GIULIO, A. & KUHLEMANN, J. (2001) Combination of single-grain fission-track chronology and morphological analysis of detrital zircon crystals in provenance studies - sources of the Macigno formation (Apennines, Italy). *Journal of Sedimentary Research*, 71, 516-525.

DUNKL, I. (2002) TRACKKEY: a Windows program for calculation and graphical presentation of fission track data. *Computers and Geosciences*. 28, 3-12.

DUNKL, I. & SZÉKELY, B. (2002) Component analysis with visualization of fitting - PopShare, a Windows program for data analysis. *Goldschmidt Conference Abstracts*, Geochim. et Cosmochim. Acta, 66/15A, 201; http://www.sediment.uni-goettingen.de/staff/dunkl/software/popshare.html

ELIAS, J. (1998) The thermal history of the Ötztal-Stubai complex (Tyrol, Austria/Italy) in the light of the lateral extrusion model. *Tübinger Geowissenschaftliche Arbeiten, Reihe A*, 36,

ELLWANGER, D., GRIMM, M., HOSELMANN, C., HOTTENROTT, M., WEIDENFELLER, M. & WIELANDT-SCHUSTER, U. (2010) Iffezheim-Formation. In: Litholex (Online-database), Record No. 1000014, Last Update: 03-11-2010. Bundesanstalt für Geowissenschaften und Rohstoffe, Hannover. http://www.bgr.bund.de/litholex (last accessed 10.01.2015.).

FARLEY, K.A., WOLF, R.A. & SILVER, L.T. (1996) The effects of long alpha-stopping distances on (U-Th)/He ages. *Geochim. et Cosmochim. Acta*, 60, 4223-4229.

FERIAKOVA, Z., MERTZ, D. F. & HOFMANN, A.W. (2007a) Geodynamic setting of the Tertiary Hocheifel volcanism (Germany), Part II: Geochemistry and Sr, Nd and Pb isotopic compositions. In: Ritter, J. R. R. and Christensen, U. R. (eds) Mantle plumes - a multidisciplinary approach. Heidelberg: Springer, pp. 207-240.

FERIAKOVA, Z., MERTZ, D. F. & HOFMANN, A.W. (2007b) Geodynamic setting of the Tertiary Hocheifel volcanism (Germany), Part I: $^{40}Ar/^{39}Ar$ geochronology. In: Ritter, J. R. R. and Christensen, U. R. (eds) Mantle plumes - a multidisciplinary approach. Heidelberg: Springer, pp. 185-206.

FISCHER, C., DUNKL, I., VON EYNATTEN, H. WIJBRANS, J.R. & GAUPP, R. (2012) Products and timing of diagenetic processes in Upper Rotliegend sandstones from Bebertal (North German Basin, Parchim Formation, Flechtingen High, Germany). *Geological Magazine*, 149, 827-840.

FREY M., DESMONS J. & NEUBAUER F. (1999) The new metamorphic map of the Alps. *Schweizerische Mineralogische und Petrographische Mitteilungen*, 79, 1-4.

GABRIEL, G., ELLWANGER, D., HOSELMANN, C., WEIDENFELLER, M., WIELANDT-SCHUSTER, U. & the Heidelberg Basin Project Team (2013) The Heidelberg Basin, Upper Rhine Graben (Germany): A unique archive of Quaternary sediments in Central Europe: *Quaternary International*. 292, 43-58.

GLASMACHER, U., ZENTILLI, M. & GRIST, A.M. (1998) Apatite Fission Track Thermochronology of Paleozoic sandstones and the Hill-Intrusion, Northern Linksrheinisches Schiefergebirge, Germany. In *Advances in Fission-Track Geochronology (Ed. by* Van den Haute & De Corte). Dordrecht, Kluwer Academic Publishers.

GLEADOW, A.J.W., HURFORD, A.J. & QUAIFE, R.D. (1976) Fission track dating of zircon: improved etching techniques. *Earth and Planetary Research Letters*, 33, 273-276.

GLEADOW, A.J.W. (1981) Fission-track dating methods: what are the real alternatives? *Nuclear Tracks*, 5, 3-14.

GLOTZBACH,C., REINECKER, J., DANIŠIK, M. RAHN, M., FRISCH, W. & SPIEGEL, C. (2008) Neogene exhumation history of the Mont Blanc massif, western Alps. *Tectonics*, 27, TC4011, doi:10.1029/2009JF001304

GRADSTEIN, F.M., OGG, J.G., & HILGEN, F.J. (2012) On the Geologic Time Scale. *Newsletters on Stratigraphy*, 45, 171-188.

GREEN, P. F. (1981) A new look at statistics in fission track dating. *Nuclear Tracks*, 5, 77-86.

GROSCHOPF, R., Kessler, G., Leiber, J., Maus, H., Ohmert, W., Schreiner, A., & Wimmenauer, W. (1996) Geologische Karte von Baden-Württemberg, 1:50.000. Erläuterungen zum Blatt Freiburg im Breisgau und Umgebung. Landesamt für Geologie, Rohstoffe und Bergbau, Baden-Württemberg, Freiburg im Breisgau.

HAGEDORN, E.-M. & BOENIGK W. (2008) The Pliocene and Quaternary sedimentary and fluvial history in the Upper Rhine Graben based on heavy mineral analyses: *Netherlands Journal of Geosciences*, 87, 21-32.

HEJL, E., COYLE, D., LAL, N., VAN DEN HAUTE, P. & WAGNER, G.A. (1997) Fission-track dating of the western border of the Bohemian massif: thermochronology and tectonic implications. *Int. J. of Earth Sci.*, 86, 210-219.

HETZEL, R., DUNKL, I., HAIDER, V., STROBL, M., VON EYNATTEN, H., DING, L. & FREI, D. (2011) Peneplain formation in southern Tibet predates India-Asia collision and plateau uplift. *Geology*, 39, 983-986.

HORTON, B.K., PARRA, M., SAYLOR, J. E. , NIE, J. , MORA., TORRES, V. , STOCKLI D.F. & STRECKER, M.R. (2010) Resolving uplift of the northern Andes using detrital zircon age signatures. *GSA Today*, 20, 4-10.

HOSELMANN, C. (2008) The Pliocene and Pleistocene fluvial evolution in the northern Upper Rhine Graben based on results of the research borehole at Viernheim (Hessen, Germany). *Quaternary Science Journal*, 57, 286-315.

HOSELMANN, C., ELLWANGER, D., GABRIEL, G., WEIDENFELLER, M. & WIELANDT-SCHUSTER, U. (2010) Viernheim-Formation. In: Litholex (Online-database), Record No.

1000013, Last Update: 03-11-2010. Bundesanstalt für Geowissenschaften und Rohstoffe, Hannover. http://www.bgr.bund.de/litholex (last accessed 10. 01.2015).

HOSKIN, P.W.O. (2005) Trace-element composition of hydrothermal zircon and the alteration of Hadean zircon from the Jack Hills, Australia. *Geochim. et Cosmochim. Acta*, 69, 637-648.

HOSKIN, P.W.O. & IRELAND, T.R. (2000) Rare earth element chemistry of zircon and its use as a provenance indicator. *Geology*, 28, 627-630.

HOURIGAN, J. K., REINERS, P. W., & BRANDON, M. T. (2005) U-Th zonation-dependent alpha-ejection in (U-Th)/He chronometry. *Geochim. et Cosmochim. Acta*, 69, 3349-3365.

HUNZIKER J.C., DESMONS J. & HURFORD A.J. (1992) Thirty-two years of geochronological work in the Central and Western Alps: a review on seven maps. *Mém. Géol. Lausanne 13*, 59pp.

HURFORD, A.J. & GREEN, P.F. (1983) The zeta age calibration of fission-track dating. *Chem. Geol*. 41, 285-312.

HURFORD, A.J., FITCH, F.J. & CLARKE, A. (1984) Resolution of the age structure of the detrital zircon populations of two Lower Cretaceous sandstones from the Weald of England by fission track dating. *Geol. Mag.*, 121, 269-277.

HURFORD, A.J. (1986) Cooling and uplift patterns in the Lepontine Alps south central Switzerland and an age of vertical movement on the Insubric fault line. *Contrib. Mineral. Petrol.*, 92, 413-427.

HURFORD, A.J., FLISCH, M. & JÄGER, E. (1989) Unravelling the thermo-tectonic evolution of the Alps: a contribution from fission track analysis and mica dating. *Geological Society, London, Special Publications*, 45, 369-398.

HURFORD, A.J. (1998) Zeta: the ultimate solution to fission-track analysis calibration or just an interim measure? in: Van den haute, P. and De Corte, F. (eds): Advances in fission-track geochronology. Kluwer Academic Publishers, pp. 19-32.

ILLIES, J. H. (1977) Ancient and Recent Rifting in the Rhinegraben: Netherland Journal of Geosciences, 56, 329-350.

JACKSON, S., PEARSON, N., GRIFFIN, W. & BELOUSOVA, E. (2004) The application of laser ablation-inductively coupled plasma-mass spectrometry to in situ U-Pb zircon geochronology. *Chemical Geology*, 211, 47-69.

KARG, H., CARTER, A., BRIX, M. R. & LITTKE, R. (2005) Late- and post-Variscan cooling and exhumation history of the northern Rhenish massif and the southern Ruhr Basin: new constraints from fission-track analysis: *Int. J. Earth Sci.* , 94, 180-192.

KEMNA, H.-A. (2005) Pliocene and Lower Pleistocene Stratigraphy in the Lower Rhine Embayment, Universität zu Köln, Diss.

KEMNA, H.-A. (2008a) Pliocene and Lower Pleistocene fluvial history of the Lower Rhine Embayment, Germany: Examples of the tectonic forcing of river courses. *Quaternary International*, 189, 106-114.

KEMNA, H.-A. (2008b) A Revised Stratigraphy for the Pliocene and Lower Pleistocene Deposits of the Lower Rhine Embayment: *Netherlands Journal of Geosciences*, 87, 91-105.

KÖPPEN, A. & CARTER, A. (2000) Constraints on provenance of the central European Triassic using detrital zircon fission track data. *Palaeogeography, Palaeoclimatology, Palaeoecology*, 161, 193-204.

KOLB, M., PAULICK, H., KIRCHENBAUR, M., & MÜNKER, C. (2012) Petrogenesis of mafic to felsic lavas from the Oligocene Siebengebirge Volcanic Field (Germany): Implications for the origin of intracontinental volcanism in Central Europe. *Journal of Petrology*, 53, 2349-2379.

KRIPPNER, A., & BAHLBURG, H. (2013) Provenance of Pleistocene Rhine River Middle Terrace sands between the Swiss-German border and Cologne based on U-Pb detrital zircon ages. *Int. J. Earth Sci.*, 102, 917-932.

LINTHOUT, K., PAULICK. H., & WIJBRANS, J.R. (2009) Provenance of basalt blocks from Roman sites in Vleuten-De Meern (the Netherlands) traced to the Tertiary Siebengebirge (Germany): a geoarchaeological quest using petrological and geochemical methods. *Netherlands Journal of Geosciences*, 88, 55-74.

LIPPOLT, H.J (1983) Distribution of volcanic activity in space and time. In: Fuchs, K., von Gehlen, K., Mälzer, H., Murawski, H. & Semmel, A. (Eds.), *Plateau Uplift: The Rhenish Shield - A Case History*. Springer, Berlin.

LITTKE, R., BAYER, U., GAJEWSKI, D., & NELSKAMP, S. (Eds) (2008) Dynamics of Complex Intracontinental Basins: The Central European Basin System. Springer, 519 p.

MANGE, M.A. & MAURER, H.F.W. (1992) Heavy Minerals in Colour. Chapman and Hall, London 148 pp.

MARTHA, S.O., ZULAUF, G., DÖRR, W., NESBOR, H-D., PETSCHICK, R., PRINZ-GRIMM, P. & GERDES, A. (2014) The Saxothuringian-Rhenohercynian boundary underneath the Vogelsberg volcanic field: evidence from basement xenoliths and U-Pb zircon data of trachyte. *German J. Geosci.*, 165, 373-394.

MCCANN, T. (Ed.), (2008) The Geology of Central Europe, Volume 1: Precambrian and Palaeozoic. Geological Society of London, 748 p.

MICHALSKI, I. & SOOM, M. (1990) The Alpine thermos-tectonic evolution of the Aar and Gotthard massifs, central Switzerland: Fission track ages on zircon and apatite and K-Ar mica ages, *Schweiz. Mineral. Petrogr. Mitt.* 70, 373-387.

MILLER, J.C. (2012) Detrital thermochronology of the Alpine foreland basin in Central Switzerland: Insights into tectonic and erosion history of the North Central Alps. *Dissertation thesis*, University of Kansas.

MORTON, A.C. & HALLSWORTH, C.R. (1994) Identifying provenance-specific features of detrital heavy mineral assemblages in sandstones. *Sedimentary Geology*, 90, 241-256.

NAESER, C.W. & Faul, H. (1969) Fission track annealing in apatite and sphene. *Journal of Geophysical Research*, 74, 705-10.

NEUHAUS, S. (2010) New age for Paleogene/Neogene clastics at the northern termination of the Upper Rhine Graben (Hesse, Germany). *German J. Geosci.*, 161, 303-322.

PAUL, J., WEMMER, K. & WETZEL, F. (2009) Keuper (Late Triassic) sediments in Germany - indicators of rapid uplift of Caledonian rocks in southern Norway. *Norwegian Journal of Geology*. 89, 193-202.

PHILLIPS, D. & MATCHAN, E.L. (2013) Ultra-high precision $^{40}Ar/^{39}Ar$ ages for Fish Canyon Tuff and Alder Creek Rhyolite sanidine: New dating standards required? *Geochim. et Cosmochim. Acta*, 121, 229-239.

RAHL J.M., REINERS, P.W., CAMPBELL, I.H., NICOLESCU, S. & ALLEN, C.M. (2003) Combined single-grain (U-Th)/He and U/Pb dating of detrital zircons from the Navajo Sandstone, Utah. *Geology*, 31, 761-764.

RAHN, M.K., BRANDON, M.T., BATT, G.E. and GARVER, J.I. (2004) A zero-damage model for fission-track annealing in zircon. *American Mineralogist*, 89, 473-484.

REINERS, P.W., SPELL, T.L., NICOLESCU, S. & ZANETTI, K.A. (2004) Zircon (U-Th)/He thermochronometry: He diffusion and comparisons with 40Ar/39Ar dating: *Geochim. et Cosmochim. Acta*, 68, 1857-1887.

REINERS, P.W. (2005) Zircon (U-Th)/He Thermochronometry. *Reviews in Mineralogy & Geochemistry*, 58, 151-179.

REITER, W., ELFERT, S., GLOTZBACH, C., BERNET, M. & SPIEGEL, C. (2013) Relations between denudation, glaciation, and sediment deposition: implications from the Plio-Pleistocene Central Alps. *Basin Research*, 25, 659-674.

ROLF, C., HAMBACH, U. & WEIDENFELLER, M. (2008) Rock and palaeomagnetic evidence for the Plio-Pleistocene palaeoclimatic change recorded in Upper Rhine Graben sediments (Core Ludwigshafen-Parkinsel). *Netherlands Journal of Geosciences*, 87, 41-50.

SCHEIDT, S., HAMBACH, U. & ROLF, C. (2015) A consistent magnetic polarity stratigraphy of late Neogene to Quaternary fluvial sediments from the Heidelberg Basin (Germany): A new time frame for the Plio-Pleistocene palaeoclimatic evolution of the Rhine Basin. *Global and Planatary Change*

SCHLUNEGGER, F., MATTER, A., BURBANK, D.W. & KLAPER, E.M. (1997) Magnetostratigraphic constraints on relationships between evolution of the central Swiss Molasse basin and Alpine orogenic events. *GSA Bulletin*, 109, 225-241.

SCHLUNEGGER & WILLETT (1999) Spatial and temporal variations in exhumation of the central Swiss Alps and implications for exhumation mechanisms. *Geological Society, London, Special Publications*, 154, 157-179.

SCHMITT, A.K., MARKS, M.A.W., NESBOR, H.D. & MARKL, G. (2007) The onset and origin of differentiated Rhine Graben volcanism based on U-Pb ages and oxygen isotopic composition of zircon. *European Journal of Mineralogy*, 19, 849-857.

SENGLAUB, Y., Brix, M.R., ADRIASOLA, A.C. & LITTKE, R. (2005) New information on the thermal history of the southwestern Lower Saxony Basin, northern Germany, based on fission track analysis. *Int. J. Earth Sci*., 94, 876-896.

SIRCOMBE (2004) AgeDisplay: an EXCEL workbook to evaluate and display univariate geochronological data using binned frequency histograms and probability density distributions. *Computers and Geosciences*, 30, 21-31.

SISSINGH, W. (2003) Tertiary paleogeographic and tectonostratigraphic evolution of the Rhenish Triple Junction. *PPP*. 196, 229-263.

SLÁMA, J., KOŠLER, J., CONDON, D.J., CROWLEY, J.L., GERDES, A., HANCHAR, J.M., HORSTWOOD, M.S.A., MORRIS, G.A., NASDALA, L., NORBERG, N., SCHALTEGGER, U., SCHOENE, B., TUBRETT, M.N. & WHITEHOUSE, M.J. (2008) Plešovice zircon - A new natural reference material for U-Pb and Hf isotopic microanalysis. *Chemical Geology* 249, 1-35.

SPIEGEL, C., KUHLEMANN, J., DUNKL, I. FRISCH, W., VON EYNATTEN, H. & BALOGH, K. (2000) The erosion history of the Central Alps: evidence from zircon fission track data of the foreland basin sediments. *Terra Nova*, 12, 163-170.

SPIEGEL C., KUHLEMANN J. & FRISCH W. (2007) Tracing sediment pathways by zircon fission track analysis: Oligocene marine connections in Central Europe. *Int. J. Earth Sci.*, 96, 363-374.

THOMSON, S.N. & ZEH, A. (2000) Fission-track thermochronology of the Ruhla Crystalline Complex: new constraints on the post-Variscan thermal evolution of the NW Saxo-Bohemian Massif. *Tectonophysics*, 324, 17-35.

TIMAR-GENG, Z., FÜGENSCHUH, B., SCHALTEGGER U. & WETZEL, A. (2004) The impact of the Jurassic hydrothermal activity on zircon fission track data from the southern Upper Rhine Graben area: Schweizerische Mineralogische und Petrographische Mitteilungen, 84, 257-269.

TIMAR-GENG, Z., FÜGENSCHUH, B., WETZEL, A. & DRESMANN, H. (2006) Low-temperature thermochronology of the flanks of the southern Upper Rhine Graben: *Int. J. Earth Sci.*, 95, 685-702.

VERMEESCH, P. (2004) How many grains are needed for a provenance study? *Earth and Planetary Science Letters*, 224, 441-451.

VERMEESCH, P. (2012) On the visualisation of detrital age distributions. *Chemical Geology*, 312-313, 190-194.

VERNON, A.J., VAN DER BEEK, P.A., SINCLAIR, H.D. & RAHN, M.K. (2008) Increase in late Neogene denudation of the European Alps confirmed by analysis of a fission-track thermochronology database. *Earth and Planetary Science Letters*, 270, 316-329.

VON EYNATTEN H. (2003) Petrography and chemistry of sandstones from the Swiss Molasse Basin: An archive of the Oligo-/Miocene evolution of the Central Alps. *Sedimentology*, 50, 703-725.

VILLINGER, E. (2003) Zur Palaeogeographie von Alpenrhein und oberer Donau: *Zeitschrift der Deutschen Geologischen Gesellschaft*, 154, 193-253.

WAGNER, G.A. (1978) Archeological applications of fission track dating. *Nuclear Track Detection*, 2, 51-63.

WALTER, R. (2007) *Geologie von Mitteleuropa*, 7th edn. Schweizerbart'sche Verlagsbuchhandlung, Stuttgart, 511 p.

WALTER, R. (2010) *Aachen und nördliche Umgebung: Sammlung Geologischer Führer*, v. 101, Gebr. Bornträger, Stuttgart, 214 p.

WEDEPOHL K.H., GOHN, E. & HARTMANN G. (1994) Cenozoic alkali basaltic magmas of western Germany and their products of differentiation. *Contrib Mineral Petrol*, 115, 253-278.

WEIDENFELLER, M. & KÄRCHER, T. (2008) Tectonic influence on fluvial preservation: aspects of the architecture of Middle and Late Pleistocene sediments in the northern Upper Rhine Graben, Germany. *Netherlands Journal of Geosciences*, 87, 33-40.

WEIDENFELLER, M. & KNIPPING, M. (2008) Correlation of Pleistocene sediments from boreholes in the Ludwigshafen area, western Heidelberg Basin. *Quaternary Science Journal*, 57, 270-285.

WESTERHOFF, W.E., KEMNA, H. A. & BOENIGK, W. (2008) The confluence area of Rhine, Meuse, and Belgian rivers: Late Pliocene and Early Pleistocene fluvial history of the northern Lower Rhine Embayment. *Netherlands Journal of Geosciences*, 87, 107-125.

WETZEL, A., R. ALLENBACH, & ALLIA, V. (2003) Reactivated basement structures affecting the sedimentary facies in a tectonically "quiescent" epicontinental basin: an example from NW Switzerland. *Sedimentary Geology*, 157, 153-172.

WIEDENBECK, M., ALLÉ, P., CORFU, F., GRIFFIN, W.L., MEIER, M., OBERLI, F., von QUADT, A., RODDICK, J.C. & SPIEGEL, W. (1995) Three natural zircon standards for U-Th-Pb, Lu-Hf, trace element and REE analyses. *Geostandards Newsletters*, 19, 1-23.

WIMMENAUER, W. (2003) *Geologische Karte von Baden-Württemberg 1:25.000. Erläuterungen zum Blatt Kaiserstuhl*. Landesamt für Geologie, Rohstoffe und Bergbau Baden-Württemberg, Freiburg im Breisgau.

WOLF, R.A., FARLEY, K.A. & SILVER, L.T. (1996) Helium diffusion and low-temperature thermochronometry of apatite. *Geochim. Cosmochim. Acta*, 60, 4231-4240.

WURSTER, P. (1964) Geologie des Schilfsandsteins. *Mitteilungen des Geologischen Staatsinstitutes Hamburg*, 13, 1-144.

ZIEGLER, P.A. (1990) Geological Atlas of Western and Central Europe, 2nd ed. Shell Internationale Petroleum Maatschappij, The Hague, 239 p.

ZIEGLER, P.A. (1992) European Cenozoic rift system. *Tectonophysics*, 208, 91-111.

ZIEGLER, P.A. & DÈZES, P. (2005) Evolution of the lithosphere in the area of the Rhine Rift System. *Int. J. Earth Sci.*, 94, 594-614.

ZIEGLER, P.A. & FRAEFEL, M. (2009) Response of drainage systems to Neogene evolution of the Jura fold-thrust belt and Upper Rhine Graben. *Swiss J. Geosci*., 102, 57-75.

Appendix Table 1: Detailed results of the single-grain U-Pb geochronology.

grain	Th/U	$^{208}Pb/^{206}Pb$	$^{206}Pb/^{238}U$	±1s [%]	$^{207}Pb/^{235}U$	±1s [%]	$^{207}Pb/^{206}Pb$	±1s [%]	rho	$^{206}Pb/^{238}U$	±2s [Ma]	$^{207}Pb/^{235}U$	±2s [Ma]	$^{207}Pb/^{206}Pb$	±2s [Ma]	Disc. I. [%]	Disc. II. [%]
P36-5																	
LU-11_64_P36-5.xl	0.338	0.125	0.08286	6.7	0.68856	12	0.06027	9.9	0.56	513.1	12.9	531.9	19.1	613.4	34.9	3.5	16.3
LU-11_65_P36-5.xl	0.479	0.178	0.16535	4.9	1.6972	8.6	0.07444	7.1	0.57	986.4	9	1008	11.2	1054	13.5	2.1	6.4
LU-11_66_P36-5.xl	0.489	0.184	0.32274	5.4	5.28732	7.9	0.11882	5.8	0.68	1803.1	9.4	1867	7.5	1939	5.4	3.4	7
LU-11_67_P36-5.xl	0.157	0.057	0.07749	4.3	0.62311	11	0.05832	9.8	0.4	481.1	8.3	491.8	17.4	541.8	39.6	2.2	11.2
LU-11_68_P36-5.xl	0.341	0.118	0.09934	4.7	0.83632	10	0.06106	8.8	0.47	610.5	9	617.1	15.3	641.3	29.5	1.1	4.8
LU-11_69_P36-5.xl	0.226	0.085	0.26848	7.1	3.84886	9.9	0.10397	7	0.71	1533.1	12.7	1603	10.4	1696	7.6	4.4	9.6
LU-11_70_P36-5.xl	0.408	0.178	0.13674	4.9	1.53843	9.7	0.0816	8.3	0.51	826.2	9.3	945.9	13	1236	13.2	12.7	33.2
LU-11_71_P36-5.xl	0.146	0.082	0.08347	4.6	0.80121	12	0.06962	10.5	0.4	516.8	8.9	597.5	17.8	917.2	23.6	13.5	43.7
LU-11_72_P36-5.xl	0.405	0.159	0.07819	3.9	0.61421	7.9	0.05698	6.9	0.5	485.3	7.6	486.2	12.8	490.6	30.8	0.2	1.1
LU-11_73_P36-5.xl	0.348	0.141	0.04893	5.1	0.27253	13	0.0404	12.3	0.38	307.9	9.9	244.7	23.9			-25.8	
LU-11_77_P36-5.xl	0.341	0.137	0.04923	4.8	0.27989	15	0.04124	14.3	0.32	309.8	9.5	250.6	27.2			-23.6	
LU-11_78_P36-5.xl	0.219	0.144	0.05425	5.0	0.40831	16	0.05459	15.4	0.31	340.6	9.7	347.7	28.2	395.5	87.6	2	13.9
LU-11_79_P36-5.xl	0.539	0.199	0.05191	5.0	0.39808	14	0.05561	13.4	0.35	326.3	9.7	340.3	24.8	437	68.3	4.1	25.3
LU-11_80_P36-5.xl	0.082	0.032	0.07724	4.5	0.60441	8.1	0.05676	6.7	0.56	479.6	8.7	480	13.1	482.1	30.9	0.1	0.5
LU-11_81_P36-5.xl	0.315	0.131	0.04852	4.8	0.36643	9.9	0.05478	8.7	0.48	305.4	9.4	317	17.2	403.2	48.2	3.7	24.3
LU-11_82_P36-5.xl	0.297	0.132	0.04693	4.0	0.35235	10	0.05445	9.5	0.38	295.6	7.7	306.5	18.1	389.9	54.9	3.5	24.2
LU-11_83_P36-5.xl	0.188	0.075	0.07382	5.0	0.58215	11	0.05719	9.8	0.46	459.2	9.7	465.8	18	499	43.3	1.4	8
LU-11_84_P36-5.xl	0.226	0.087	0.08412	6.0	0.6902	11	0.05951	8.7	0.57	520.7	11.6	532.9	16.8	585.8	32.1	2.3	11.1
LU-11_88_P36-5.xl	0.556	0.219	0.40325	5.9	9.53067	8.4	0.17141	6	0.7	2184	10	2391	6.7	2572	3.9	8.6	15.1
LU-11_89_P36-5.xl	0.23	0.083	0.07818	5.4	0.64695	11	0.06001	9.9	0.47	485.3	10.3	506.6	18.2	604.1	35.6	4.2	19.7
LU-11_90_P36-5.xl	0.197	0.086	0.07434	4.7	0.58574	10	0.05714	9.2	0.46	462.3	9.2	468.1	16.9	497.1	40.6	1.3	7
LU-11_91_P36-5.xl	0.443	0.208	0.05248	5.3	0.27617	15	0.03817	13.7	0.36	329.7	10.4	247.6	26.5			-33.2	
LU-11_92_P36-5.xl	0.204	0.087	0.07762	5.2	0.60926	11	0.05693	10.1	0.46	481.9	10.1	483.1	18.5	488.7	45.5	0.2	1.4
LU-11_93_P36-5.xl	0.333	0.137	0.05451	4.8	0.37546	9	0.04995	7.6	0.54	342.2	9.4	323.7	15.6	192.9	91.1	-5.7	-77.4
LU-11_94_P36-5.xl	0.071	0.022	0.07316	4.7	0.58988	9.4	0.05848	8.1	0.5	455.2	9.2	470.8	15.3	547.7	32.5	3.3	16.9

grain	Th/U	$^{208}Pb/^{206}Pb$	$^{206}Pb/^{238}U$	±1s [%]	$^{207}Pb/^{235}U$	±1s [%]	$^{207}Pb/^{206}Pb$	±1s [%]	rho	$^{206}Pb/^{238}U$	±2s [Ma]	$^{207}Pb/^{235}U$	±2s [Ma]	$^{207}Pb/^{206}Pb$	±2s [Ma]	Disc. I. [%]	Disc. II. [%]
Z-P36-5-006.FIN2	0.204	0.076	0.07734	1.3	0.62136	1.8	0.05827	1.3	0.7	480.2	11.6	490.7	14	539.9	28.4	2.1	11
Z-007.FIN2	0.372	0.119	0.13397	2.6	1.28227	2.9	0.06942	1.2	0.91	810.5	40.1	837.9	33.3	911.3	25.5	3.3	11.1
Z-008.FIN2	0.267	0.089	0.0728	1.0	0.55404	1.9	0.05519	1.5	0.57	453	9.2	447.6	13.4	420.1	34.4	-1.2	-7.8
Z-009.FIN2	0.596	0.2	0.31098	2.3	5.10607	2.5	0.11908	1.1	0.9	1745.5	70.5	1837	43.6	1943	20.3	5	10.1
Z-010.FIN2	0.364	0.122	0.09209	0.7	0.75352	1.7	0.05935	1.5	0.41	567.9	7.4	570.3	14.5	579.9	33.3	0.4	2.1
Z-011.FIN2	0.189	0.109	0.13061	3.2	1.62992	3.6	0.09051	1.7	0.88	791.3	47.1	981.8	45.6	1436	32.5	19.4	44.9
Z-012.FIN2	0.719	0.246	0.1175	2.0	1.03798	2.5	0.06407	1.5	0.8	716.1	27.2	722.9	26.2	744.1	32.3	0.9	3.8
Z-013.FIN2	0.506	0.162	0.13047	1.3	1.17486	1.9	0.06531	1.4	0.67	790.5	19.3	788.9	21.4	784.4	30.8	-0.2	-0.8
Z-014.FIN2	0.511	0.178	0.07283	1.1	0.56812	1.7	0.05658	1.3	0.62	453.2	9.3	456.8	12.5	475.1	29.7	0.8	4.6
Z-015.FIN2	0.446	0.154	0.0432	0.9	0.30076	1.8	0.05049	1.6	0.48	272.6	4.7	267	8.7	217.7	37.8	-2.1	-25.2
Z-021.FIN2	0.669	0.231	0.05017	1.1	0.36284	1.7	0.05245	1.4	0.62	315.6	6.6	314.3	9.4	305.1	31.3	-0.4	-3.4
Z-022.FIN2	0.417	0.15	0.04229	0.9	0.30204	2	0.0518	1.8	0.43	267	4.5	268	9.6	276.8	42.4	0.4	3.5
Z-023.FIN2	0.417	0.141	0.04377	1.0	0.31296	2.1	0.05186	1.9	0.47	276.2	5.3	276.5	10.2	279.3	42.7	0.1	1.1
Z-024.FIN2	0.472	0.169	0.05402	1.5	0.39515	2.3	0.05305	1.7	0.64	339.2	9.6	338.1	13.1	331	39.8	-0.3	-2.5
Z-025.FIN2	0.08	0.029	0.07089	0.8	0.54985	1.5	0.05625	1.2	0.58	441.5	7.2	444.9	10.5	462.4	26.7	0.8	4.5
Z-026.FIN2	0.041	0.014	0.07181	1.0	0.55128	1.6	0.05568	1.2	0.62	447	8.4	445.8	11.3	439.7	27.6	-0.3	-1.7
Z-027.FIN2	0.235	0.083	0.04549	0.8	0.33002	1.7	0.05262	1.6	0.46	286.8	4.5	289.6	8.8	312.4	35.6	1	8.2
Z-028.FIN2	0.092	0.031	0.06969	0.9	0.54139	1.6	0.05634	1.3	0.57	434.3	7.8	439.3	11.7	465.9	30.1	1.1	6.8
Z-029.FIN2	0.242	0.086	0.10092	3.0	1.02299	3.9	0.07352	2.5	0.77	619.8	35.6	715.4	40.8	1028	51.4	13.4	39.7
Z-030.FIN2	0.401	0.149	0.35516	4.5	8.16412	4.7	0.16672	1.2	0.96	1959.2	154.3	2249	87	2525	22	12.9	22.4
Z-036.FIN2	0.205	0.072	0.07265	1.0	0.55202	1.7	0.05511	1.3	0.61	452.1	8.8	446.3	12.1	416.6	29.9	-1.3	-8.5
Z-037.FIN2	0.157	0.055	0.07195	1.0	0.55323	1.8	0.05576	1.5	0.57	447.9	8.7	447.1	12.9	443.1	32.8	-0.2	-1.1
Z-038.FIN2	0.311	0.111	0.05725	0.9	0.43203	2	0.05473	1.8	0.47	358.9	6.6	364.6	12.3	401.3	39.8	1.6	10.6
Z-039.FIN2	0.402	0.145	0.05144	0.9	0.38774	1.6	0.05467	1.2	0.6	323.4	5.9	332.7	8.8	398.6	28.2	2.8	18.9
Z-040.FIN2	0.258	0.085	0.07409	1.0	0.57683	1.7	0.05646	1.4	0.6	460.8	9.2	462.4	12.9	470.7	31.1	0.4	2.1
Z-041.FIN2	0.73	0.257	0.09096	1.4	0.76011	1.9	0.06061	1.4	0.7	561.2	14.7	574.1	17.1	625.3	30.1	2.2	10.2
Z-042.FIN2	0.134	0.068	0.08535	2.1	0.82788	2.7	0.07035	1.7	0.76	528	20.8	612.4	24.9	938.6	36.1	13.8	43.7
Z-043.FIN2	0.155	0.054	0.06992	1.0	0.54053	1.8	0.05607	1.5	0.56	435.7	8.5	438.8	12.8	455.2	33.3	0.7	4.3
Z-044.FIN2	0.978	0.336	0.15872	0.8	1.57282	1.4	0.07187	1.1	0.57	949.6	14	959.5	17.3	982.3	23.7	1	3. 3

grain	Th/U	$^{208}Pb/^{206}Pb$	$^{206}Pb/^{238}U$	±1s [%]	$^{207}Pb/^{235}U$	±1s [%]	$^{207}Pb/^{206}Pb$	±1s [%]	rho	$^{206}Pb/^{238}U$	±2s [Ma]	$^{207}Pb/^{235}U$	±2s [Ma]	$^{207}Pb/^{206}Pb$	±2s [Ma]	Disc. I. [%]	Disc. II. [%]
HAM-1																	
Z-045.FIN2	0.19	0.064	0.04182	1.1	0.2962	1.9	0.05136	1.6	0.57	264.1	5.6	263.4	9	257.3	36.8	-0.3	-2.7
Z-HAM1-006.FIN2	0.866	0.313	0.00416	5.0	0.01711	52	0.02983	51.6	0.1	26.8	2.7	17.2	17.8			-55.3	
Z-007.FIN2	0.408	0.134	0.05887	1.4	0.45235	2.9	0.05573	2.5	0.5	368.8	10.2	378.9	18.1	441.6	55.3	2.7	16.5
Z-008.FIN2	1.255	0.4	0.00376	3.1	0.02543	16	0.04904	15.3	0.2	24.2	1.5	25.5	7.9	149.8	359	5.1	83.8
Z-009.FIN2	0.913	0.317	0.00401	2.7	0.03011	8.7	0.0544	8.3	0.31	25.8	1.4	30.1	5.2	387.8	185	14.3	93.3
Z-010.FIN2	0.832	0.295	0.05181	1.3	0.37462	3	0.05244	2.7	0.43	325.6	8	323.1	16.4	304.8	61	-0.8	-6.8
Z-011.FIN2	0.749	0.244	0.05744	1.1	0.42052	2.4	0.05309	2.2	0.47	360.1	8	356.4	14.7	332.8	49.1	-1	-8.2
Z-012.FIN2	2.225	0.749	0.00392	2.0	0.01893	8.4	0.03502	8.2	0.24	25.2	1	19	3.2			-32.5	
Z-013.FIN2	0.616	0.192	0.44697	1.2	9.95511	1.7	0.16154	1.2	0.68	2381.8	45.9	2431	31.6	2472	22.1	2	3.6
Z-014.FIN2	0.718	0.249	0.00427	3.9	0.01892	33	0.03211	32.7	0.12	27.5	2.1	19	12.5			-44.4	
Z-015.FIN2	0.78	0.259	0.00439	5.2	0.03573	26	0.05907	25.1	0.2	28.2	2.9	35.6	18	569.6	547	20.8	95
Z-021.FIN2	0.827	0.275	0.00379	1.7	0.02563	5.7	0.04906	5.5	0.3	24.4	0.8	25.7	2.9	150.9	128	5.1	83.8
Z-022.FIN2	0.961	0.322	0.00399	2.6	0.02614	9.2	0.04751	8.8	0.28	25.7	1.3	26.2	4.8	75.1	209	2	65.8
Z-023.FIN2	0.64	0.156	0.00419	5.2	0.01851	43	0.03203	42.5	0.12	27	2.8	18.6	15.8			-44.8	
Z-024.FIN2	0.882	0.274	0.05278	1.3	0.40898	3.3	0.0562	3	0.4	331.6	8.7	348.1	19.7	460.4	67.7	4.8	28
Z-025.FIN2	0.631	0.198	0.0042	3.2	0.02189	21	0.03785	20.6	0.15	27	1.7	22	9.1			-22.7	
Z-026.FIN2	1.089	0.358	0.09733	1.1	0.81891	2.5	0.06102	2.2	0.45	598.7	13	607.4	23	640.2	48.1	1.4	6.5
Z-027.FIN2	0.638	0.21	0.07974	1.2	0.61898	2.1	0.0563	1.7	0.56	494.6	11.1	489.2	16.2	464.3	38.5	-1.1	-6.5
Z-028.FIN2	0.792	0.303	0.00427	3.8	0.03065	15	0.05207	14.1	0.26	27.5	2.1	30.7	8.8	288.5	323	10.4	90.5
Z-029.FIN2	1.071	0.262	0.00465	4.5	0.03507	27	0.05476	26.5	0.17	29.9	2.7	35	18.6	402.5	593	14.6	92.6
Z-030.FIN2	1.826	0.618	0.00386	1.6	0.0266	4.5	0.04997	4.2	0.35	24.8	0.8	26.7	2.4	193.9	98.4	6.8	87.2
Z-036.FIN2	1.745	0.641	0.00364	2.8	0.03484	11	0.06936	10.3	0.27	23.4	1.3	34.8	7.3	909.4	212	32.6	97.4
Z-037.FIN2	1.205	0.616	0.0039	3.5	0.02251	17	0.04181	16.7	0.21	25.1	1.8	22.6	7.6			-11.2	
Z-038.FIN2	0.363	0.119	0.05381	1.2	0.39985	2.4	0.0539	2.1	0.51	337.9	8.1	341.5	14.1	366.8	47.3	1.1	7.9
Z-039.FIN2	0.836	0.257	0.00428	5.4	0.02303	35	0.03901	34.7	0.15	27.5	2.9	23.1	16.1			-19.1	
Z-040.FIN2	0.645	0.262	0.00401	5.7	0.04674	31	0.08459	30	0.19	25.8	3	46.4	27.9	1306	583	44.4	98
Z-041.FIN2	0.538	0.175	0.00406	6.1	0.00448	294	0.008	294	0.02	26.1	3.2					-475.5	
Z-042.FIN2	0.951	0.301	0.00419	3.2	0.01748	26	0.03028	25.7	0.12	26.9	1.7	17.6	9.1			-53.1	

grain	Th/U	$^{208}Pb/^{206}Pb$	$^{206}Pb/^{238}U$	±1s [%]	$^{207}Pb/^{235}U$	±1s [%]	$^{207}Pb/^{206}Pb$	±1s [%]	rho	$^{206}Pb/^{238}U$	±2s [Ma]	$^{207}Pb/^{235}U$	±2s [Ma]	$^{207}Pb/^{206}Pb$	±2s [Ma]	Disc. I. [%]	Disc. II. [%]
Z-043.FIN2	0.584	0.195	0.05256	1.2	0.38666	3.1	0.05336	2.9	0.38	330.2	7.6	331.9	17.9	344	66	0.5	4
Z-044.FIN2	0.332	0.112	0.0699	1.2	0.53788	2.7	0.05581	2.4	0.43	435.6	9.7	437	19.3	444.8	54.4	0.3	2.1
Z-045.FIN2	0.71	0.232	0.05222	1.2	0.39206	2.7	0.05445	2.4	0.45	328.2	7.8	335.9	15.5	389.7	54.4	2.3	15.8
Z-051.FIN2	0.27	0.089	0.07416	1.1	0.55935	2.3	0.0547	2	0.48	461.2	9.8	451.1	16.8	400.1	45.2	-2.2	-15.3
Z-052.FIN2	1.08	0.365	0.07591	1.3	0.60293	2.5	0.0576	2.2	0.51	471.7	11.9	479.1	19.5	514.8	48	1.5	8.4
Z-053.FIN2	0.264	0.086	0.31135	1.1	4.57538	2.2	0.10658	1.9	0.5	1747.3	34.1	1745	37.8	1742	36.2	-0.1	-0.3
Z-054.FIN2	0.684	0.313	0.07897	1.6	1.00243	7.2	0.09206	7	0.23	490	15.4	705	74.7	1469	134	30.5	66.6
Z-055.FIN2	0.069	0.025	0.07337	1.0	0.55736	2.1	0.0551	1.8	0.5	456.4	9	449.8	15	416.1	40.1	-1.5	-9.7
Z-056.FIN2	0.665	0.218	0.09232	1.0	0.73878	1.8	0.05804	1.5	0.54	569.3	10.7	561.7	15.8	531.3	34	-1.3	-7.1
Z-057.FIN2	1.098	0.413	0.004	2.7	0.02578	11	0.04677	10.8	0.24	25.7	1.4	25.8	5.7	37.6	257	0.5	31.6
Z-058.FIN2	0.843	0.326	0.00416	4.4	0.02646	26	0.04608	25.2	0.17	26.8	2.4	26.5	13.4			-1	
Z-059.FIN2	1.037	0.384	0.00384	3.5	0.02079	20	0.03932	19.5	0.18	24.7	1.7	20.9	8.2			-18.1	
Z-060.FIN2	0.923	0.305	0.09832	1.0	0.80985	1.7	0.05974	1.4	0.57	604.6	11.4	602.4	15.9	594.2	31.5	-0.4	-1.7
Z-066.FIN2	0.419	0.152	0.05704	1.0	0.45758	2.8	0.05819	2.7	0.34	357.6	6.7	382.6	18.2	536.8	58.5	6.5	33.4
Z-067.FIN2	0.416	0.136	0.08902	1.0	0.72187	2.6	0.05881	2.4	0.39	549.7	10.9	551.8	22.5	560.3	53	0.4	1.9
Z-068.FIN2	1.207	0.429	0.00403	3.4	0.02903	16	0.05227	15.6	0.21	25.9	1.8	29.1	9.2	297.2	355	10.8	91.3
Z-069.FIN2	0.245	0.205	0.09682	1.0	1.43875	2.3	0.10777	2	0.46	595.8	11.7	905.2	27.3	1762	37.2	34.2	66.2
Z-070.FIN2	1.208	0.402	0.00435	2.3	0.02071	15	0.03455	14.6	0.15	28	1.3	20.8	6.1			-34.3	

U and Pb content and Th/U ratio were calculated relative to GJ-1 reference zircon.

$^{207}Pb/^{235}U$ calculated using $^{207}Pb/^{206}Pb/(^{238}U/^{206}Pb*1/137.88)$

rho is the $^{206}Pb/^{238}U/^{207}Pb/^{235}U$ error correlation coefficient.

discordance I = (1 - ($^{206}Pb/^{238}U$) age / ($^{207}Pb/^{235}U$) age) * 100

discordance II = (1 - ($^{206}Pb/^{238}U$) age / ($^{207}Pb/^{206}Pb$) age) * 100